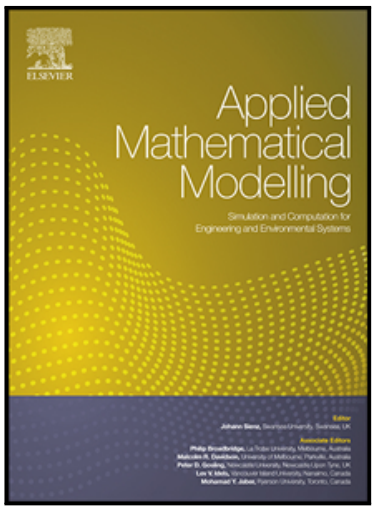

Numerical modelling of 3D sloshing experiments in rectangular tanks

Laura Battaglia, Marcela Cruchaga, Mario Storti, Jorge D'Elía,
Jonathan Núñez Aedo, Ricardo Reinoso

PII: S0307-904X(18)30045-3
DOI: 10.1016/j.apm.2018.01.033
Reference: APM 12149

To appear in: *Applied Mathematical Modelling*

Received date: 19 April 2017
Revised date: 25 January 2018
Accepted date: 30 January 2018

Please cite this article as: Laura Battaglia, Marcela Cruchaga, Mario Storti, Jorge D'Elía, Jonathan Núñez Aedo, Ricardo Reinoso, Numerical modelling of 3D sloshing experiments in rectangular tanks, *Applied Mathematical Modelling* (2018), doi: 10.1016/j.apm.2018.01.033

Highlights

- Improved mass-preserving renormalization method for 3D two-fluid viscous flows
- Report of new 3D experimental data for free-surface evolution in sloshing problems
- 3D confirmation of 2D predictions for free and forced sloshing planar modes
- Experimental validation for simulation of fully 3D sloshing cases
- Effect of the initial conditions on the 3D simulation

Numerical modelling of 3D sloshing experiments in rectangular tanks

Laura Battaglia[a,b,*], Marcela Cruchaga[c], Mario Storti[a], Jorge D'Elía[a], Jonathan Núñez Aedo[c], Ricardo Reinoso[c]

[a] *Centro de Investigación de Métodos Computacionales (CIMEC), UNL-CONICET, Predio CONICET Santa Fe "Dr. Alberto Cassano", Colectora Ruta Nac. Nro 168, Km 0, Paraje El Pozo, Santa Fe, Argentina*
[b] *Grupo de Investigación de Métodos Numéricos en Ingeniería (GIMNI), Univ. Tecnológica Nacional, Facultad Regional Santa Fe, Lavaise 610, Santa Fe, Argentina*
[c] *Departamento de Ingeniería Mecánica, Universidad de Santiago de Chile (USACH). Av. Bdo. O'Higgins 3363, Santiago de Chile, Chile*

Abstract

This work encompasses numerical and experimental studies of three-dimensional (3D) sloshing problems. The two-fluid viscous flow, which is solved within a stabilized finite element context, involves liquid and gaseous phases. The free surface is captured with a level set (LS) method, including the bounded renormalization with continuous penalization technique, to avoid the well-known spreading of the marker function. Specifically, this technique is improved with a volume-preserving algorithm for long-term analyses. To verify the numerical model, the responses of free-sloshing cases are compared with analytical solutions and other results computed using a Lagrangian technique. These simulations assess the influence of considering two-dimensional (2D) and 3D analyses, as well as the effects of depth and viscosity. This work presents data obtained from a forced sloshing experiment that is specifically devoted to 3D free surface behaviour. free surface evolution measurements are used to validate the numerical method. Moreover, the effect of the initial conditions used to promote 3D behaviour in the modelling is evaluated.

Keywords: sloshing experiments, finite elements, level set, 3D

*Correspondign Author
Email address: lbattaglia@santafe-conicet.gov.ar (Laura Battaglia)

volume-preserving, bounded renormalization, continuous penalization

1. Introduction

The sloshing problem is relevant to the analysis of liquid transportation [1], the study of the effect of vibrations on liquid storage tanks [2, 3] or liquid damper devices [4, 5], and many other engineering applications. Several methods have been developed to study and predict free surface behaviour, such as experimental studies, analytical solutions, and numerical methods [6, 7, 8, 9, 10].

Typical analytic solutions for sloshing problems are given in terms of potential flow theory, assuming incompressible and inviscid fluid flow. Different approaches can be distinguished. For example, low order asymptotic mathematical theories [8] and multimodal or pseudospectral methods that describe nonlinear sloshing of irrotational flow have been derived in a general form in [11] and later applied to several tank shapes and fluid flow depths [12, 13, 14, 15].

Numerical methods are a powerful tool to computationally solve the equations involved in the fluid dynamics of free surface flow problems. Many efforts have been made to develop efficient algorithms to describe moving interfaces, and different versions of very well known techniques are available to properly describe long-term free surface problems. The volume of fluid [16, 17, 9, 18], level set (LS) [19, 20], Eulerian-Lagrangian [21, 22, 23], and deforming domain [24, 25] methods have been proposed to describe interface motions in the framework of different discretization schemes, i.e., finite differences, finite volumes, or finite element formulations. In addition, several techniques, such as smooth particle hydrodynamics [26], particle finite elements [27], and boundary elements [28], have been specifically developed or have been successfully applied to describe free surface flow problems [29]. Hybrid or mixed techniques have been also proposed for two-phase flows, as coupled LS and VOF methods [30, 31, 32, 33] or the particle level set method [34], among others [35, 36] Moreover, a relevant task in modeling is the validation of simulations by contrasting their computed results with experiments, such as those reported for the

sloshing problem in [17, 37, 25, 23, 18, 38].

The basis of the LS technique is the use of a continuous scalar field to identify the two phases. The interface between theses phases (or a free surface) is represented by a certain value of the scalar function. The interface motion is controlled by an advection equation of the scalar field. To avoid a loss of quality in the numerical solution when solving such an equation, the scalar field must be renormalised at the interface surroundings. To this end, a distance function is used in the original LS works [39]. In addition, a smoothed properties distribution is commonly adopted to describe the jump in the material properties at the interface. Different LS techniques have been proposed in the literature with different proposals adopted to solve the main drawbacks [29, 40]. The volume change in the phases involved in an LS approach is a known issue that often leads to errors in the interface position [41, 42] and promotes large distortions in the results for long-term simulations. Several strategies have been proposed to maintain the volume of each phase in an LS [42, 43]. Additionally, some conservative LS methods have been developed with the specific aim of conserving mass in two-fluid flow simulations [44, 45]. The local mass-preserving strategy presented by Ausas et al. [20] can be taken as a reference. Other numerical free surface capturing methods also make use of global mass controls [46].

The present work focuses on the analysis of 3D sloshing problems within the context of a finite element formulation using an improved renormalization for the LS technique. In particular, this investigation proposes a bounded renormalization with continuous penalization (BRCP) technique [47, 48] improved with a mass-preserving algorithm to avoid the loss of mass in 3D analyses. The formulation is applied to the simulation of free and forced 3D sloshing problems. Moreover, a set of repeatable forced sloshing experiments is conducted to describe the free surface evolution under different imposed motion. The imposed external amplitudes and frequencies vary within a range to promote primary and secondary resonance modes. The evolution of the 3D behaviour is also described as a function of the imposed parameters. The results of this experiment are fully reported here to provide valuable data to evaluate the simulations.

Two representative cases of 3D sloshing are simulated to assess the performance of the described methodology. The influence of the initial conditions on the 3D responses is also evaluated.

The main contributions of this work can be summarized as:

- improved mass-preserving bounded renormalization technique
- new experimental results focused on 3D sloshing behaviour
- analytic free-sloshing model verification
- experimental validation for 3D sloshing models
- confirmation of 2D predictions for planar mode responses of sloshing with 3D simulations
- effect of the initial conditions on the 3D simulation
- experimental validation of the modelling of fully 3D sloshing modes.

The remainder of this paper is organized as follows. The governing equations and a short description of the related discrete formulation are presented in Section 2. Section 3 reports the LS technique proposed and used in the analyses of the studied sloshing problems. This section also includes a short description of a Lagrangian interface technique (MLIRT) [49, 50] used as an alternative method to compare the computed numerical results. Free-sloshing analyses are reported in Section 4 to compare the analytical and numerical results for both deep and shallow water conditions. Section 5 presents the forced sloshing analyses that encompass the experimental (5.1) and numerical studies (5.2).

2. Fluid flow governing equations

The methods for solving free surface flows in this context are proposed such that both a liquid phase and an incompressible gaseous phase, separated by an interface, coexist in a single fluid domain Ω. The fluid flow is described by the

incompressible Navier-Stokes equations for time $t \in [0, T]$, where T is the final time point, as follows,

$$\rho\left(\mathbf{u}_t + \mathbf{u}\cdot\nabla\mathbf{u} - \mathbf{g}\right) - \nabla\cdot\boldsymbol{\sigma} = \mathbf{0} \text{ in } \Omega, \tag{1}$$

$$\nabla\cdot\mathbf{u} = 0 \text{ in } \Omega, \tag{2}$$

where $\mathbf{u}$ is the fluid velocity, ρ is the fluid density, $\mathbf{g}$ is the body force per unit density, and $\boldsymbol{\sigma} = \boldsymbol{\sigma}(\mathbf{u}, p)$ is the fluid stress tensor. The time derivative is denoted by the subindex t, and ∇ represents the gradient. The Newtonian stress tensor is adopted, so

$$\boldsymbol{\sigma} = -p\mathbf{I} + \mathbf{T}, \tag{3}$$

where p is the pressure, $\mathbf{I}$ is the identity tensor, and $\mathbf{T} = 2\mu\boldsymbol{\epsilon}(\mathbf{u})$ is the deviatoric component of $\boldsymbol{\sigma}$. The dynamic viscosity is μ, and the strain rate is given by

$$\boldsymbol{\epsilon}(\mathbf{u}) = \frac{\mathbf{1}}{\mathbf{2}}(\nabla\mathbf{u} + \nabla^{\mathbf{T}}\mathbf{u}). \tag{4}$$

The interface between the two fluids is described by additional equations aimed at predicting the interface position over time, and in turn to define the fluid properties distribution in space. These issues are summarized in Sections 3.1 and 3.2.

The boundary conditions for solid boundaries defined as $\partial\Omega = \Gamma$ are given as

$$\mathbf{u} = \mathbf{u}_{\mathrm{D}} \qquad \text{on } \Gamma_{\mathrm{D}}\ , \tag{5}$$

$$\boldsymbol{\sigma}\cdot\mathbf{n} = \mathbf{t} \qquad \text{on } \Gamma_t\ , \tag{6}$$

where Γ_{D} is the Dirichlet component of the contour and Γ_t the Neumann component, taking into account that $\Gamma = \Gamma_{\mathrm{D}} \cup \Gamma_t$ and $\Gamma_{\mathrm{D}} \cap \Gamma_t = \emptyset$.

The governing equations are solved using stabilized finite element formulations for both of the applied numerical methods. For the LS approach, streamline upwind/Petrov–Galerkin (SUPG) [51] and pressure-stabilizing/Petrov-Galerkin (PSPG) [24] are implemented, as described in [52]. For details about stabilization when solving the free surface with MLIRT, see [53].

3. Free surface description

3.1. Improved interface capturing technique

A continuous function ϕ, or level set function, is used to determine which of the two phases is present at each point of the domain [39]. Specifically, for every spatial coordinate $\mathbf{x}$ in the fluid domain Ω in time t,

$$\phi(\mathbf{x},t)\begin{cases} >0 & \text{if} \quad \mathbf{x}\in\Omega_l, \\ =0 & \text{if} \quad \mathbf{x}\in\Gamma_{\mathrm{I}}, \\ <0 & \text{if} \quad \mathbf{x}\in\Omega_g, \end{cases} \tag{7}$$

i.e., $\mathbf{x}$ belongs either to the liquid (denser) phase Ω_l or to the incompressible gaseous (lighter) phase Ω_g, with $\Omega=\Omega_l\cup\Omega_g$ and $\Omega_g=\Omega\backslash\Omega_l$. Moreover, the interface between such phases is $\Gamma_{\mathrm{FS}}=\{\mathbf{x}|\phi(\mathbf{x},t)=0\}$.

The solution of the NS equations, described in Sec. 2, has to consider the variation of fluid properties, which are defined as a function of ϕ,

$$\eta(\phi)=\frac{1}{2}\left[\left(1+\tilde{H}(\phi)\right)\eta_l+\left(1-\tilde{H}(\phi)\right)\eta_g\right], \tag{8}$$

where $\eta(\phi)$ is either the density $\rho(\phi)$ or the dynamic viscosity $\mu(\phi)$. In the present approach, the LS function is bounded to $-1\leq\phi\leq 1$ and $\tilde{H}(\phi)$ is a smoothed sign function, $\tilde{H}(\phi)=\tanh\left(\frac{\pi\phi}{\tilde{\varepsilon}}\right)$, where $\tilde{\varepsilon}$ is a parameter that controls the transition width from the positive to the negative region.

The LS function ϕ, defined over the whole domain Ω, is driven by the fluid velocity $\mathbf{u}$, which is obtained from the NS equations solution,

$$\partial_t\phi+\mathbf{u}\cdot\nabla\phi=0, \tag{9}$$

where the boundary condition can be given as $\phi=\bar{\phi}$ on only inflow sections $\Gamma_{\mathrm{in}}=\{\Gamma|\ \mathbf{u}\cdot\mathbf{n}<0\}$.

3.1.1. Renormalization algorithm

The regularity of the function ϕ is preserved with the bounded renormalization with continuous penalization (BRCP) technique [47], which consists of

solving the following equation over domain Ω,

$$\phi\ (\phi^2 - \phi_{\text{ref}}^2) - \kappa\Delta\phi + M\left(\hat{H}(\phi) - \hat{H}(\phi_0)\right) = 0, \tag{10}$$

where ϕ_0 is the LS function value obtained by solving Eq. (9). The reference value is adopted as $\phi_{\text{ref}} = 1$, κ is a numerical diffusive parameter, and M is a penalty coefficient. Typical values of parameter κ are from h^2 to $(3h)^2$, where h is the element size, and M is adopted as $O(10^{n_{\text{d}}+2})$, where n_{d} is the number of spatial dimensions to solve. Note that although parameters κ and M are chosen by tunning, they are bounded by the element size and space dimensions, limiting the range of values to be used. Finally, the continuous function $\hat{H}(\phi) = \tanh(2\pi\phi)$ is used for the penalizing term.

The solution of Eq. 10 provides a distribution of function ϕ at the interface that is different from the distance function defined in the original LS technique, see, e.g., [39]. Other proposals that appeal to bounded marking functions are those known as the conservative level set (CLS) method [54, 44], where $0 \leq \phi \leq 1$ [55, 56, 45], and the edge-tracked interface locator technique (ETILT) [57].

3.1.2. 3D volume preservation technique

In order to overcome the mass loss problem, an explicit volume-preserving strategy has been implemented in the context of the BRCP. This procedure has previously been applied to 2D cases [40] and is assessed for 3D problems in the present work.

The volume-preserving procedure consists of correcting the field $\hat{\phi}_{n+1}$, which is the level set function obtained from the BRCP procedure in time step $n+1$, as follows,

$$\phi_{n+1} = \hat{\phi}_{n+1} + \Delta\phi_{n+1}, \tag{11}$$

i.e., the mass correction procedure sums $\Delta\phi_{n+1}$ to the LS function field, such that the interface identified with $\phi = 0$ is displaced. The volume variation in each time step is $\Delta V = V_{n+1} - V_0$, in which the initial volume of the liquid (denser) phase is V_0 and V_{n+1} is the liquid phase volume in time step $n+1$. In each time step, ΔV can be distributed along the free surface extension L_{FS} as

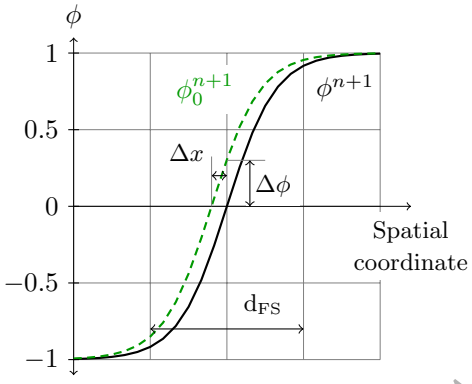

Figure 1: Schematic representation of parameters involved in the volume-conservation scheme.

$\Delta V = L_{\mathrm{FS}}\ \Delta x$, where Δx is the free surface spatial displacement that forces volume conservation. Regarding the parameters available in each time step, as shown in Fig. 1, the gradient can be approximated as

$$\nabla\phi \approx \frac{\Delta\phi}{\Delta x} \approx \frac{2\phi_{\mathrm{ref}}}{d_{\mathrm{FS}}}, \tag{12}$$

where d_{FS} is the transition width related to the diffusivity parameter of Eq. (10), such that $d_{\mathrm{FS}} = \kappa^{1/2}$. Then,

$$\Delta\phi \approx \frac{2\phi_{\mathrm{ref}}\ \Delta x}{\kappa^{1/2}} = \frac{2\phi_{\mathrm{ref}}\ \Delta V}{\kappa^{1/2} L_{\mathrm{FS}}}. \tag{13}$$

By defining the parameter $D_{\mathrm{vol}} = \frac{1}{2} L_{\mathrm{FS}} \kappa^{1/2}$ and considering an explicit numerical procedure, then

$$\Delta\phi_{n+1} = C_{\mathrm{vol}}\ D_{\mathrm{vol}}^{-1}\,(V_{n+1} - V_0)\,, \tag{14}$$

where the dimensionless coefficient C_{vol} controls the stability of the scheme and is generally set to $C_{\mathrm{vol}} = 0.1$.

Note that L_{FS} is a mean extension of the interface that is adopted at the beginning of the analysis, and is a length in 2D fluid flow cases and an area in 3D cases. Taking into account the fact that κ is given, D_{vol} is easily determined from the data of typical problems.

Finally, the LS numerical approach that is applied to the 3D sloshing problems consists of three numerical stages that are solved for each time step of the simulation:

i. the NS equations for the fluid flow domain Ω;

ii. the transport of the LS function ϕ;

iii. the reinitialization of ϕ to maintain the regularity of the function and the volume of the phases.

The performance of the numerical method without the mass-conserving stage have been satisfactorily evaluated for short-term 2D and 3D test problems, encompassing the transport and reinitialization of the LS function [47] as well as free surface fluid flows [48]. From the analysis of these results, it was concluded that mass loss is not relevant for such short-term problems. Moreover, the mass-preserving methodology has been previously assessed for 2D cases [40] for long-term analysis.By contrast, the present investigation focused on the analysis of the volume-preserving algorithm for long-term 3D problems.

LS techniques are successfully applied in the literature to describe breaking waves, where specific drop or bubble models can be included to properly describe the physics of the problem. In the present work, specific effort is made to compare the experimental and numerical results for 3D sloshing cases. The described technique is applied to the 3D nonlinear description of an experimental sloshing problem, specifically to quantify the free surface position with high-twist distortion.

3.2. Moving Lagrangian Interface Remeshed Technique [MLIRT]

This alternative technique to track moving interfaces on a fixed mesh is briefly described below for completeness of the work. In the present study, this technique is applied to verify the formulation proposed in Sec. 3.1 together with analytical solutions, which have not been previously reported (see Sec.4). MLIRT includes mass correction, subelement integration, and interface remeshing. It was reviewed in [40], and additional subjects are found in the references

mentioned therein. Experiments and simulations assessing the capabilities of this technique to solve 2D sloshing problems have been reported in [23].

In this technique, the interface is described by markers with coordinates $\mathbf{X}$ that move from time n to $n+1$ according to

$$\mathbf{X}_{n+1} = \mathbf{X}_n + \delta t \ \mathbf{V}_{n+\theta}, \tag{15}$$

where θ is the time integration parameter (usually set to 1.0), δt is the time step, $\mathbf{V}_{n+\theta}$ is the velocity of the marker, and $\mathbf{X}_{n+1}$ is its current position. The velocity of a marker is computed by interpolating the velocity field at the position of the marker. To this end, an algorithm to identify the element that hosts the marker is also included. The interface position at time $n+1$, represented by the markers with updated coordinates $\mathbf{X}_{n+1}$, must be volume preserving for incompressible flows. To ensure this aspect, an algorithm to compute the volume-preserving coordinates $\mathbf{X}_{n+1}^{\mathrm{vol-pres}}$ at time $n+1$ was proposed in [50] based on the following criterion:

$$\mathbf{X}_{n+1}^{\mathrm{vol-pres}} = \mathbf{X}_{n+1} + \beta \delta \mathbf{X}, \tag{16}$$

where $\delta \mathbf{X}$ is chosen to satisfy the mass fluxes along the interface of unit normal $\mathbf{n}$ as $\delta \mathbf{X} = -\mathrm{sign}(\mathbf{V}\cdot\mathbf{n})\mathbf{V}\delta t$, and β is the minimum parameter computed to fulfill the condition $(n_{\mathrm{d}})^{-1} \int_{\Gamma_l} (\mathbf{X}_{n+1}^{\mathrm{vol-pres}} \cdot \mathbf{n}) \mathrm{d}\Gamma_l = V_{\mathrm{known}}$, where n_{d} is the number of spatial dimensions considered, Γ_l is the boundary of the current Ω_l, and V_{known} is the volume to be preserved (see reference [50] for further details).

The basic flowchart of the process can be summarized as:

1. distribute the material properties according to the current interface position;
2. solve the Navier-Stokes equations in the entire Ω using a subelement integration technique to properly capture discontinuities in the properties;
3. update the interface using Eq. (15);
4. apply the volume correction Eq. (16) to the updated interface;
5. remesh the interface based on preserving curvatures techniques to avoid distortions (as reported in [49] and [50] for 2D and 3D cases, respectively);

6. go to 1.

Remark: Each time the markers move, a geometric algorithm is required to check whether they are inside the domain. If a marker is outside the domain, it is recovered on the boundary, and the volume correction and remeshing algorithms are applied to promote a new admissible distribution of markers.

4. Free sloshing tests

In the present work, free sloshing problems are presented to validate the reported 3D numerical technique in comparison with simulations obtained using MLIRT [49, 50] and the analytic solution. The influence of the liquid depth on the free surface evolution is also assessed.

A closed container with dimensions $0.8\,\mathrm{m} \times 0.3\,\mathrm{m} \times a$ (with $a = 2.00\,\mathrm{m}$ and $a = 0.60\,\mathrm{m}$, for deep and shallow two-fluid flows, respectively) is filled with two liquids, the lighter on top of the heavier, as shown in Fig. 2(a).

The following examples can be considered as benchmarks to verify two-fluid flow formulations. In fact, linearized analytic solutions can be found for deep water conditions, e.g., see [58]. In addition, previous numerical solutions [59, 60, 49, 50] can be taken as references for shallow-water conditions. In this context, a y-acceleration of g = -0.294 m/s^2, which is not taken from physical experiments, is adopted (as in the analysis reported in [59]). Moreover, these examples does not consider turbulent effects because the Reynolds number of the flow is low.

4.1. Deep two-fluid free sloshing

The analytic solution of the proposed numerical example was presented in [58] considering linearized analysis of a viscous incompressible two-phase flow of infinite depth and lateral distance. The model using $a = 2\,\mathrm{m}$ represents deep-water conditions, i.e., negligible effects of the top and bottom walls can be considered, as in the analytic solution. The initial position of the free surface is a half-length sinusoidal representing the first sloshing mode, as shown in Fig. 2(b),

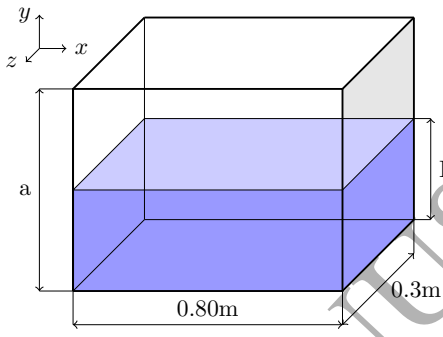

(a) Geometry

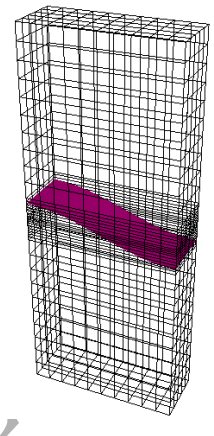

(b) Deep two-fluid

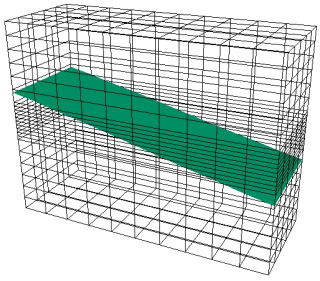

(c) Shallow two-fluid

Figure 2: Free sloshing tests. Sketch of the container, finite element discretizations and initial conditions.

given by the expression $h(x) = -h_0 \sin\left(\pi \frac{x-2}{x_{\mathrm{M}}}\right)$, where $h_0 = 0.10$ m is the initial maximum amplitude of the free surface, and $x_{\mathrm{M}} = 0.8$ m is the width of the tank. The analytical solution for the linearized case of free oscillation of a two-fluid flow, where both fluids have the same kinematic viscosity ν, is valid for small-amplitude flat waves in an infinite depth domain. This solution is given in [58] as

$$h(t) = \frac{4(1-4\beta)\nu^2 k^4}{8(1-4\beta)\nu^2 k^4 + {\omega_0}^2}\ h_0\ \mathrm{erfc}(\nu k^2 t)^{1/2} + \sum_{i=1}^{4} \frac{z_i}{Z_i}\left(\frac{\omega_0^2 h_0}{z_i^2 - \nu k^2}\right) \exp[(z_i^2 - \nu k^2)t]\ \mathrm{erfc}(z_i t^{1/2})\ , \tag{17}$$

where k is the wave number, $\omega_0^2 = gk$ is the inviscid natural frequency, and $\beta = \rho_l \rho_g/(\rho_l + \rho_g)^2$ is a dimensionless parameter that is zero in one-fluid cases. Each z_i is the root of the following algebraic equation

$$z^4 - 4\beta(k^2\nu)^{1/2} z^3 + 2(1-6\beta)k^2\nu z^2 + 4(1-3\beta)(k^2\nu)^{3/2} z + (1-4\beta)\nu^2 k^4 + \omega_0^2 = 0\ , \tag{18}$$

where $Z_1 = (z_2 - z_1)(z_3 - z_1)(z_4 - z_1)$, resulting in Z_2, Z_3, and Z_4 by circular permutation of the indices, and erfc(...) is the error function for complex variables.

The densities are $\rho_l = 2\ \mathrm{kg\ m^{-3}}$ for the lower fluid and $\rho_g = 1\ \mathrm{kg\ m^{-3}}$ for the upper fluid. Moreover, the dynamic viscosities are given as $\mu_l = 0.002\ \mathrm{kg\ (m\ s)^{-1}}$ and $\mu_g = 0.001\ \mathrm{kg\ (m\ s)^{-1}}$ for the denser (lower) and lighter (upper) fluids, respectively. The depth is $D = a/2 = 1\,\mathrm{m}$, see Fig. 2(a). Perfect slip conditions are chosen over all the walls, and the boundary condition for pressure is $p = 0$ on one node of the top of the domain.

For both MLIRT and LS+BRCP, the mesh is composed of hexahedral elements of constant width in the $x-$ and $z-$directions, with 10 elements and 5 elements in the $x-$ and $z-$directions, respectively. By contrast, there are three element sizes in the $y-$direction: 10 layers of regular elements of height $h_{ey} = 0.088$ m in the lower and the top 0.88 m regions, each followed by 6 layers of $h_{ey} = 0.013$ m toward the middle of the domain, and 4 layers of $h_{ey} = 0.01$ m in the central region, see Fig. 2(b).

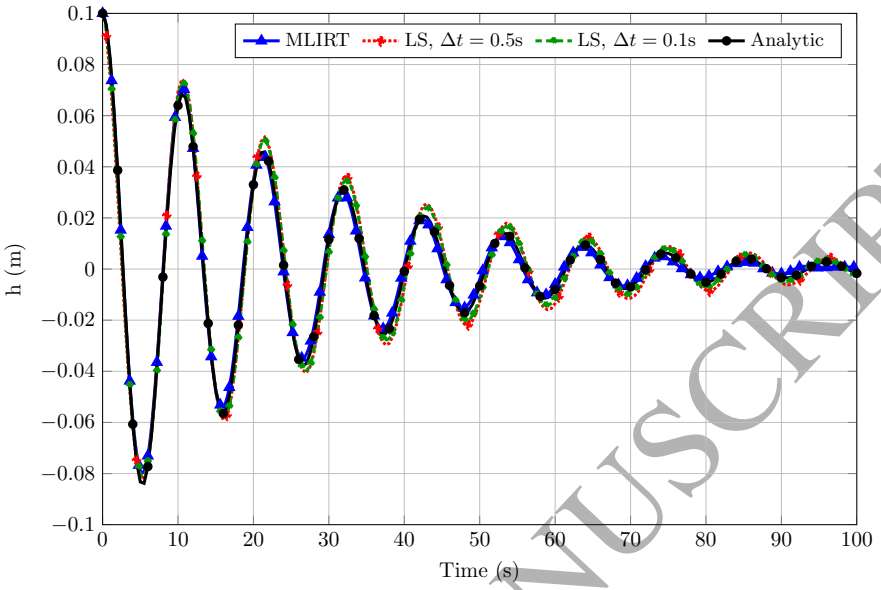

Figure 3: Deep two-fluid free sloshing problem. Comparison of the numerical results with the analytic solution and MLIRT.

The parameters for the numerical resolution using LS+BRCP are $\kappa = (3h_y)^2 = 0.0009$ m^2, considering $h_y = 0.01$ m measured in the neighborhood of the free surface, and $M = 50000$ for the renormalization procedure, with $C_{\text{vol}} = 0.1$ and $D_{\text{vol}} = 0.3$ m $\times$ 0.8 m $\times \kappa^{1/2} = 0.0072$ m^3 for the volume control algorithm.

The time history of the wave height h is reported in Figure 3, where the analytical solution is plotted with three numerical results: LS+BRCP solved with $\Delta t = 0.1$ s and $\Delta t = 0.5$ s, and MLIRT with $\Delta t = 0.1$ s.

The numerical results obtained with LS+BRCP show an acceptable free surface evolution curve; however, the amplitudes are slightly higher than expected, regardless of the time step. On the other hand, MLIRT shows better performance, which may be attributable to the fact that the interface is explicitly represented by the markers, leading to higher precision in the determination of the displacement.

Regarding the effectiveness of the volume-conserving strategy and taking the

results obtained with LS+BRCP using a time step $\Delta t = 0.1\,\mathrm{s}$ and $C_{\mathrm{vol}} = 0.1$ as a reference, the results show volume variations bounded by 0.15% of the original denser-phase volume. When $C_{\mathrm{vol}} = 0$, the denser phase loses 0.2% of its volume. Although this magnitude is relatively low, the free surface position at rest should be 1.00 m, and it is reduced by 2 mm at time $t = 120\,\mathrm{s}$. Therefore, the error with respect to wave height h_0 is 2%, and it increases with time. When time step is $\Delta t = 0.5\,\mathrm{s}$ and $C_{\mathrm{vol}} = 0.1$, the volume variation is also less than 0.15%. For the same time step without volume control, the liquid loss is 0.5% and the free surface is 5 mm lower than expected at time $t = 120\,\mathrm{s}$. In short-term analyses, the mass loss is negligible; however, for long-term simulations with numerous oscillating periods, the volume change becomes unacceptable.

4.2. Shallow two-fluid flow free sloshing

The free sloshing problem in a rectangular tank has been extensively reported in several papers to assess the numerical behaviour of different proposed formulations, see, e.g., [59, 60, 49, 50].

The effect of the water depth on the free surface evolution is assessed at two fluid depth values $D = a/2$, in two different domains with the same side lengths of 0.80 m and 0.30 m in the $x-$ and $z-$directions, respectively, see Fig. 2(a).

The fluid densities are $\rho_l = 2$ kg m^{-3} and $\rho_g = 1$ kg m^{-3} for the bottom and the top fluids, respectively. The dynamic viscosity is the same for both fluids, $\mu = 0.001$ kg (m s)$^{-1}$.

The initial condition for the example is a plane inclined 14° from the rest position, giving a maximum displacement amplitude of $h_0 = 0.10$ m. The boundary conditions for the NS problem are perfect slip on the vertical walls and no slip ($\mathbf{u} = 0$) over the bottom of the domain.

The domain is discretized in hexahedral elements of uniform size of 0.10 m in the $x-$direction, and 0.06 m in the $z-$direction, whereas in the y-direction, there is a bottom region of 6 layers of elements with a height of 0.04 m, a middle region of 10 elements with a height of 0.012 m, and a top region with 6 layers with a height of 0.04 m, see Fig. 2(c).

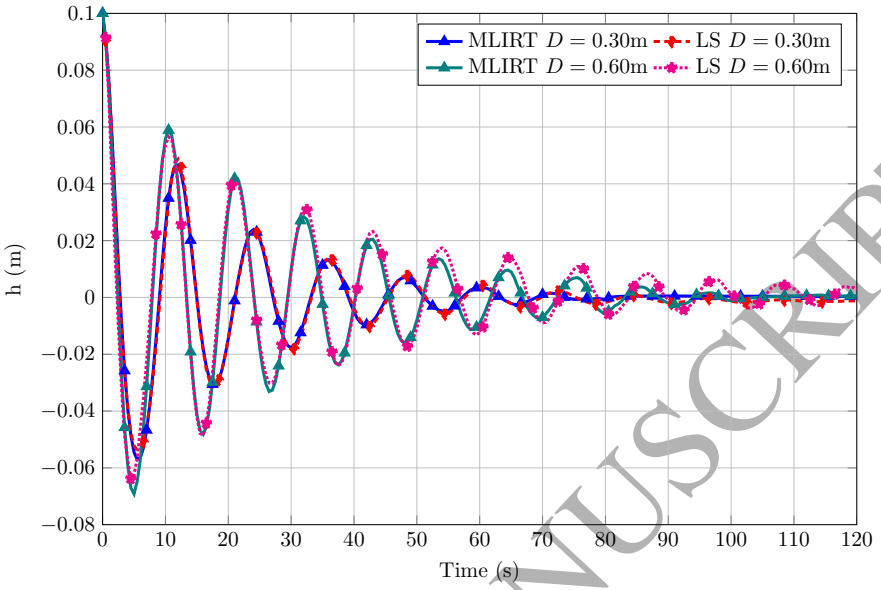

Figure 4: Shallow free sloshing problem. free surface position on the left wall of the domain for different fluid depths and numerical methods.

For the LS+BRCP procedure, the renormalization parameters are $\kappa = (3h_y)^2 = 0.001296$ m^2 and $M = 50000$, and the volume control coefficients are $C_{\text{vol}} = 0.1$ and $D_{vol} = 0.3$ m $\times$ 0.8 m $\times \kappa^{1/2} = 0.00864$ m^3.

The influence of the liquid depth D on the amplitude and period of the waves can be seen in Fig. 4, where the wave amplitude evolution is plotted for depths $D_1 = 0.30$ m and $D_2 = 0.60$ m in the problem solved with MLIRT and LS+BRCP. As the depth increases, the period decreases and the amplitude decays at a slower rate.

The free surface evolution is shown in Fig. 5 for the case with $D_1 = 0.30$m, where the 2D-like behaviour of the system is seen. The selected time points are the approximate minimum and maximum displacements for the first two periods of the simulation.

The results obtained with LS+BRPC for depths D_1 and D_2 show volume variations less than 0.4% during the simulation.

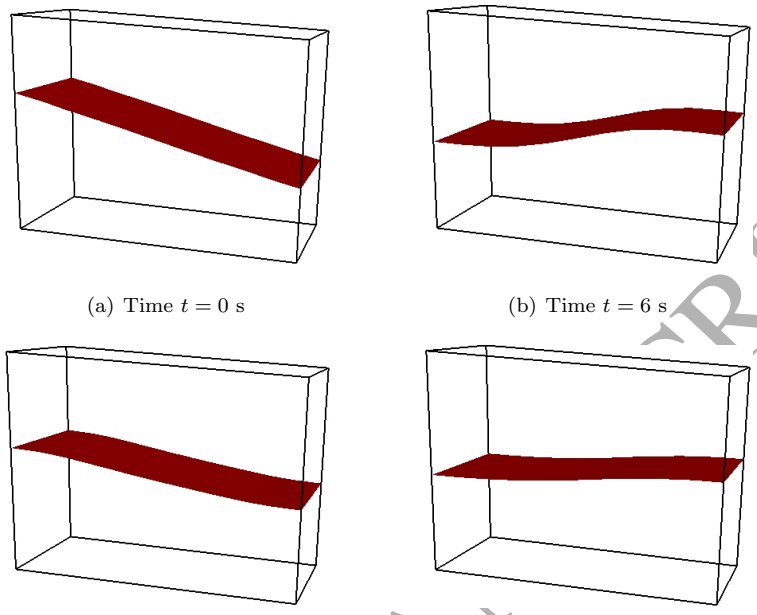

(a) Time $t = 0$ s (b) Time $t = 6$ s

(c) Time $t = 12$ s (d) Time $t = 18$ s

Figure 5: free surface evolution for the shallow free sloshing case with $D_1 = 0.30$m solved with LS+BRCP.

5. Forced sloshing tests

5.1. Experimental work

The analysed sloshing problem consist of an acrylic tank with rectangular cross section (aspect ratio 2:1) mounted on a shake table.

The tank is a parallelepiped with a width of $L_x = 0.388$ m, a depth of $L_z = 0.183$ m, and a height of $L_y = 0.30$ m. Assuming potential flow and an incompressible fluid, the natural frequencies can be analytically determined [61] as

$$\omega_{i,j}^2 = \frac{g}{L_x}\pi\left(i^2 + s^2 j^2\right)^{1/2} \tanh\left[\pi\left(i^2 + s^2 j^2\right)^{1/2} \frac{D}{L_x}\right], \tag{19}$$

where i and j are the indices associated with the $x-$ and $z-$directions, respectively; $s = L_y/L_x$ is the aspect ratio of the tank; and D is the filling depth. Table 1 summarizes the lower frequencies $f_{i,j} = \omega_{i,j}/2\pi$ associated with the first modes in the analysed tank, which is filled with water up to $D = 100\,\text{mm}$.

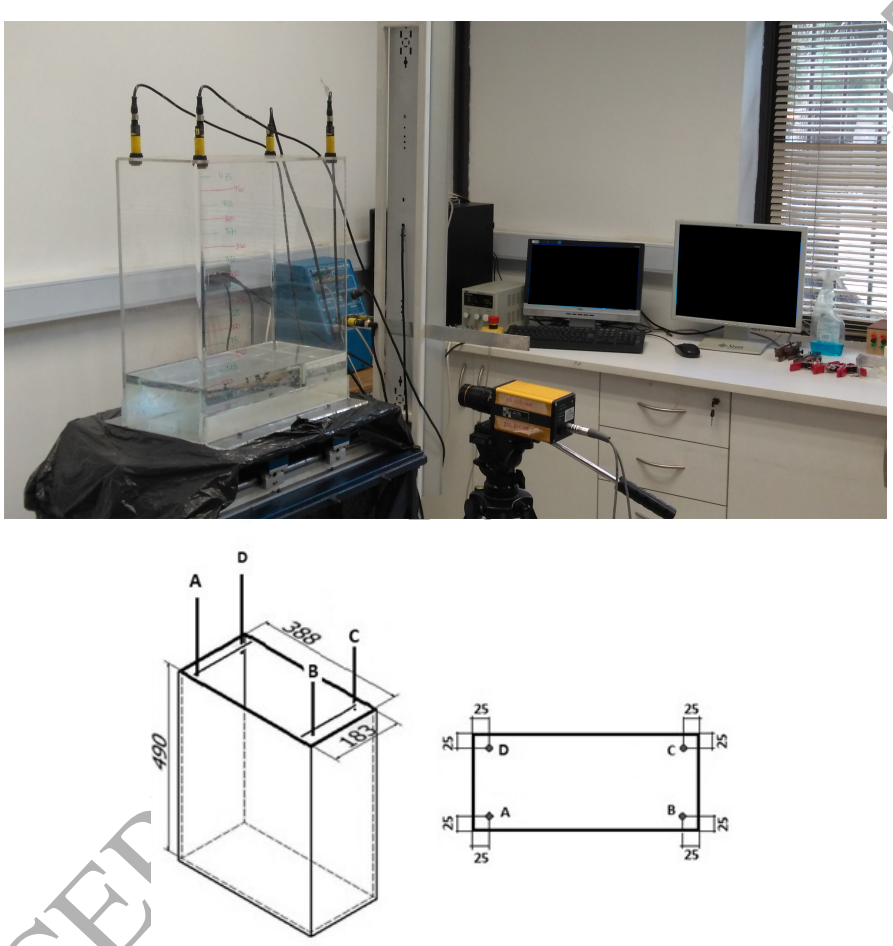

Figure 6: Experimental layout (top), position of sensors and tank dimensions (bottom) in mm, error ±1 mm.

The tank is subjected to controlled single harmonic (one-directional) motion. The experimental layout was originally reported in [23], where only 2D sloshing behaviour was analysed. The present study is focused on the 3D response that appears at certain frequencies and amplitudes of the sinusoidal waveform imposed during forced vibration, particularly near resonance conditions. Figure 6 shows the experimental set up of the shake table loaded with the instrumented tank, table controllers, and ultrasonic sensors, together with the dimensions of the tank and the sensor positions placed to properly capture the 3D free surface evolution. The experiments were also video recorded. The analysis of the videos confirms the data obtained from the sensors. A discrete sweep-frequency analysis from 0.58 Hz to 2.80 Hz is performed using imposed shaking motion of amplitudes of 2.5 mm, 5 mm, 7.5 mm, and 10 mm. Figure 7 summarizes the maximum and minimum wave heights computed for the different experiments during the time-periodic forced vibration regime (only for the signal registered by the sensor located at point A). In such a figure, the frames are used to illustrate the 2D and 3D effects. The frames are taken from the experiments where the sloshing modes clearly evolve, i.e., they are not obtained for the same imposed amplitude. The sensor measurements have an experimental bounded error of 0.5 mm as a maximum, and the sample frequency is 1000 data points per second.

Modes							
i	1	2	0	1	2	3	3
j	0	0	1	1	1	0	1
$f_{i,j}$ [Hz]	1.1605	1.9288	1.9998	2.1235	2.4001	2.4378	2.7116

Table 1: First natural frequencies for the 3D domain.

The occurrence of 3D sloshing modes strongly depends on the imposed amplitudes and frequencies, e.g., strong 3D patterns evolve near resonance at mode (1,0) for higher imposed amplitudes, which also increases the frequency range at which such effects are detected. By contrast, the water level evolution is well captured near frequency (1,0) by sensors for imposed amplitudes less than 5

mm because the free surface motion is nearly 2D at frequencies close to 1.16 Hz. For imposed amplitudes of 7.5 mm and 10 mm near 1.16 Hz, disorder evolves and the maximum and minimum wave heights cannot be properly determined, i.e., from 1.08 Hz to 1.26 Hz, 3D swirling and diagonal-like motion modes are obtained for an imposed amplitude of 10 mm. The second mode (2,0) appears during the experiments at 1.91 Hz. This mode is clearly defined for imposed amplitudes of 7.5 mm and 10 mm. Note that the free surface levels at the sensor's locations are not significant for all imposed amplitudes. The sloshing mode (1,1) evolves at a frequency of 2.1 Hz and its 3D pattern can be observed at an imposed amplitude of 5 mm. For greater imposed amplitudes, the 3D flows exhibit a more complex wave pattern. Specifically, the sloshing at frequency of 2.1 Hz with an imposed amplitude of 10 mm, is reported in the present work as a benchmark. The obtained experimental data, wave height, and frequencies at the different control points are reported along with numerical predictions in Section 5.2.2. Finally, mode (2,1) can be detected only for a small imposed amplitude of 2.5 mm at 2.4 Hz. Higher imposed amplitudes at such frequencies induce unstable 3D motion.

Two cases are selected from the described set of experiments for 3D simulations, i.e., sloshing under imposed motion of amplitude $A = 10$ mm with frequencies:

- $f_1 = 0.87$ Hz promoting 2D motion near the primary vibration mode, which was previously solved only in 2D domains [23, 40]. It is presented in this work to confirm the free surface behaviour throughout a 3D analysis.
- $f_2 = 2.10$ Hz, which has not been previously reported and is adopted here to validate the 3D numerical method.

5.2. Modelling the experiments

The present analysis encompasses the study of an imposed motion of amplitude 10 mm at two frequencies, $f_1 = 0.87$ Hz and $f_2 = 2.10$ Hz, which promote

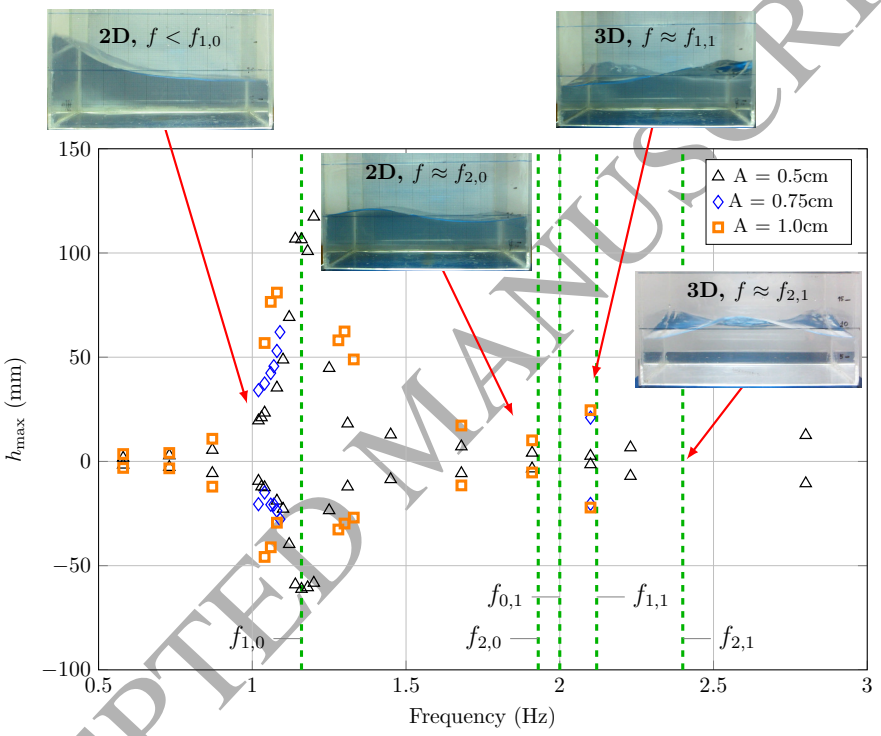

Figure 7: free surface behaviour as a function of the imposed frequency f and shake amplitude A.

2D and 3D free surface responses, respectively. The computational domain covers the tank geometry depicted in Figure 6.

The sloshing at $f_1 = 0.87\,\text{Hz}$ reported in [23, 40] is taken as a reference solution for the 3D analysis proposed in the present work. Moreover, the numerically obtained 3D results confirm the 2D assumption adopted in the referenced works and the related experimental observations. The numerical solution of the sloshing at 2.10 Hz has not been previously reported, and is considered here to validate the 3D results.

Slip boundary conditions for the NS problem are imposed over the lateral and top walls, and non-slip velocity conditions are applied to the bottom. The pressure is set to zero on one node of the top of the domain. As previously mentioned, the movement is induced by horizontal acceleration with amplitude 10 mm and frequency $f_1 = 0.87$ Hz or $f_2 = 2.10$ Hz, while vertical acceleration corresponds to gravity $g = -9.81$ m s^{-2} in the y-direction.

The simulations are conducted with the following fluid properties: $\rho_1 = 998.2$ kg m^{-3} and $\mu_1 = 0.001$ kg (m s)$^{-1}$ for water and $\rho_2 = 1.225$ kg m^{-3} and $\mu_2 = 0.000018$ kg (m s)$^{-1}$ for air.

Several studies have applied turbulence modelling to sloshing cases, see, e.g., [62], and the references therein. Turbulence dissipation near the interface has a strong influence on the free surface displacements and has to be accounted for [62]. Furthermore, turbulence models numerically help to moderate disorder at the free surface level and accounts for jumps in the fluid properties [63]. In these analyses, a simple turbulence model is adopted, which consists of using $\mu_t = \min(\mu + l_{\text{mix}}^2 \rho \sqrt{2\boldsymbol{\epsilon} : \boldsymbol{\epsilon}}, \mu_{\max})$, instead of μ, where the parameters to be given are the mixing length l_{mix} and the cutoff value $\mu_{\max}$. For the numerical resolution with finite elements, the mixing length is proposed as $l_{\text{mix}} = C_{\text{t}} h_{\text{UGN}}$, where C_{t} is a model parameter and h_{UGN} is an element length given as in [24]. This model has been successfully applied and experimentally validated for two-fluid flows, as in the case of the collapse of fluid columns [64, 57, 40] and sloshing problems [23, 40].

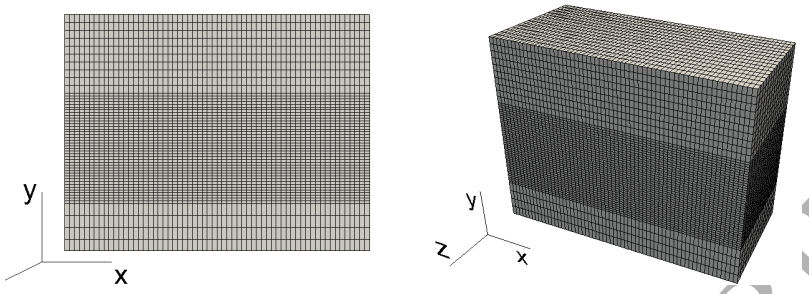

(a) Two-dimensional mesh. (b) Three-dimensional mesh.

Figure 8: Finite element discretization for forced sloshing cases.

5.2.1. Sloshing with an imposed frequency of $f_1 = 0.87$ Hz

The domain is discretized into uniform hexahedral elements: 62 in the x-direction, 15 in the z-direction, and 54 in the y-direction, see Fig 8(b). The mesh is refined in the neighborhood of the interface, in the vertical direction, where there are 40 layers of elements with a height of 0.0035 m, a bottom region of 4 layers with a height of 0.015 m and a top region of 10 layers with a height of 0.01 m.

The 2D domain used to check the two-dimensional behaviour of the 0.87 Hz case is a rectangular box with a width of $L_x = 0.388$ m and a height of $L_y = 0.30$ m, which has been discretized with linear quadrangular elements and the same number of elements in the $x-$ and y-directions as in the 3D model, see Fig. 8(a). All the 3D and 2D simulations are performed using time steps of $\Delta t = 0.01$ s. The turbulent dissipation is taken into account considering $l_{\text{mix}} = 0.15$ m, with a cutoff value for the viscosity of $\mu_{\max} = 0.10$ kg (m s)$^{-1}$.

LS+BRCP requires different but equivalent parameters for the 2D and 3D cases [47]. The 2D analysis is solved with $M = 1000$ and $\kappa = (3h_y)^2 = 1.1 \times 10^{-4}$ m^2, with $C_{\text{vol}} = 0.1$ and $D_{\text{vol}} = L_x(3h_y) = 4.07 \times 10^{-3}$ m^2 for the volume-conservation scheme. The 3D case is analysed using $M = 10000$ and $\kappa = (3h_y)^2 = 1.1 \times 10^{-4}$ m^2, adopting $C_{\text{vol}} = 0.1$ and $D_{\text{vol}} = L_x\ L_z\ (3h_y) = 7.66 \times 10^{-4}$ m^3 for volume conservation.

The fluid is initially at rest, i.e., the uniform depth of $D = 0.10$ m and zero

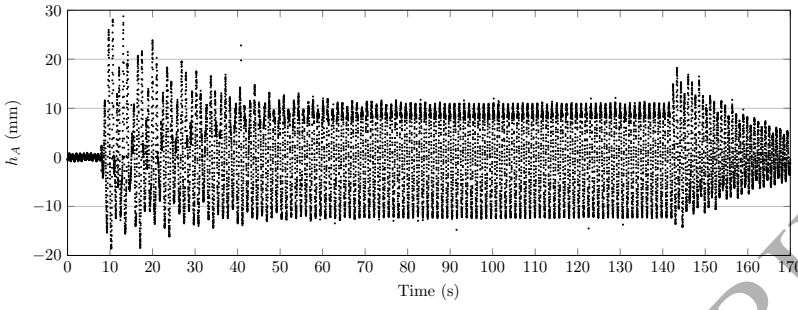

Figure 9: Forced sloshing with $f = 0.87\,\mathrm{Hz}$. Experimental register for sample A.

velocities on the whole domain.

A horizontal acceleration of amplitude $A = 10$ mm and frequency $f_1 = 0.87\,\mathrm{Hz}$ is applied from time $T_0 = 0$ to time $T = 140$ s; then, the system evolves under free sloshing until $T = 170$ s. Figure 9 shows the experimentally determined free surface evolution at point A, located as shown in Fig. 6. The numerical solutions obtained by LS+BRCP in the 2D and 3D domains, as well as the results from MLIRT 2D are plotted in Fig. 10. The 2D and 3D solutions almost coincide, and small discrepancies can be observed between the two numerical methods.

A time-periodic sloshing regime is registered after the initial transient stage. The computed free surface evolution is plotted in Fig. 11, which shows good agreement between the numerical responses and the experimental data. The signals registered by the sensors at control points A and D (as well as at points B and C) practically coincide, indicating a lack of 3D effects. The signals at control points A(D) and B(C) are shifted half a period in time. This experimentally observed behaviour is also found in the numerical analysis. The numerical differences are bounded for the maximum admissible numerical error, i.e., half of the element size.

Figure 12 shows snapshots of the free surface at two instants during the time-periodic regime, where 2D-like behaviour is apparent. The free surface presents curvature evolution in the plane xy only, as shown in Fig. 13. This fact

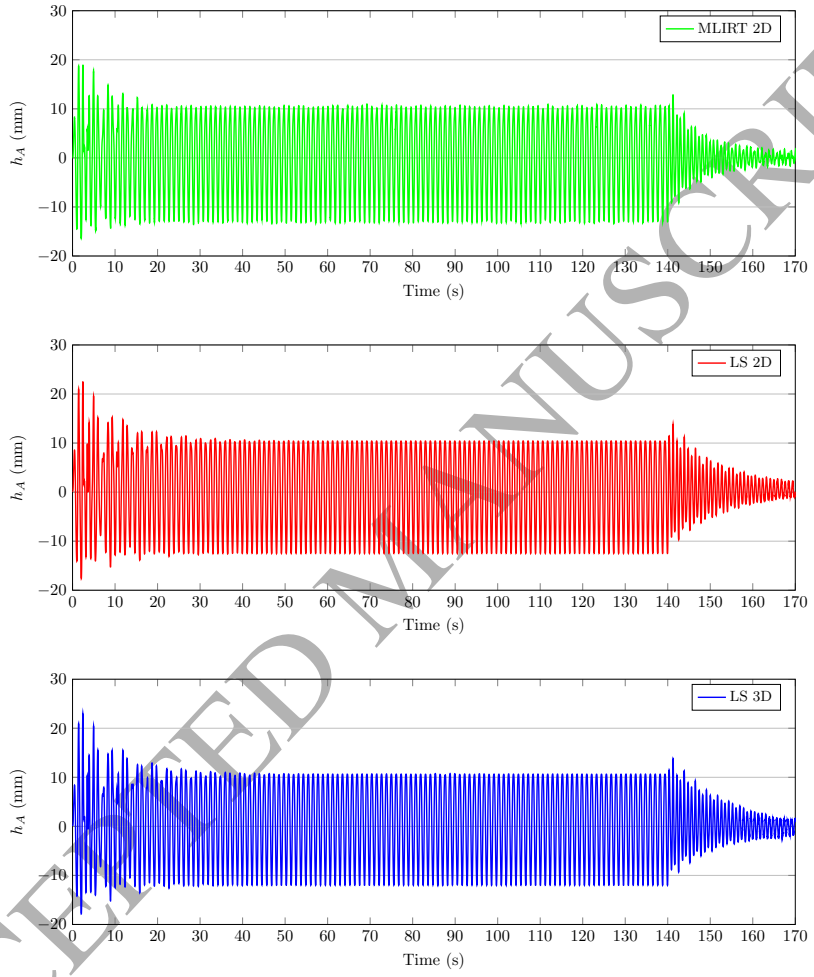

Figure 10: Forced sloshing with $f = 0.87\,\text{Hz}$. Total time evolution for sample A determined with different numerical strategies in 2D and 3D. From top to bottom: MLIRT 2D, LS 2D and LS 3D, respectively.

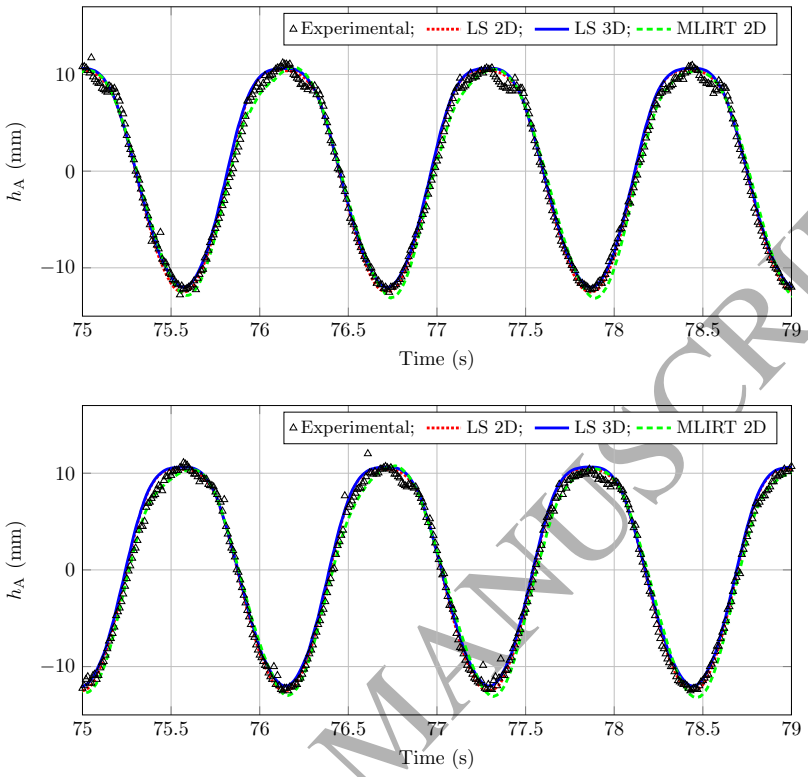

Figure 11: Forced sloshing with $f = 0.87$ Hz. Experimental and numerical results for free surface evolution during time-periodic sloshing at points A (top) and B (bottom).

is confirmed by the nearly coincident signals registered by the sensors at control points A and D and by the sensors at control points B and C, as is reported in [65]. Moderate maximum wave amplitudes near 10% of the water depth are observed.

The volume-preserving algorithm performance has been evaluated with respect to cases with time and spatial refinement, with and without mass control, considering the percentage of volume variation of the water ΔV_w in time $t = 100$ s, i.e., for 10000 time steps. The results presented thus far are taken as a reference, with $C_{vol} = 0.1$, time step $\Delta t = 0.01$ s and vertical mesh size $h_{FS} = 3.5$ mm measured in the refined region of the domain and summarized in Table 2. The water loss is reduced with a reduction in the time step and no

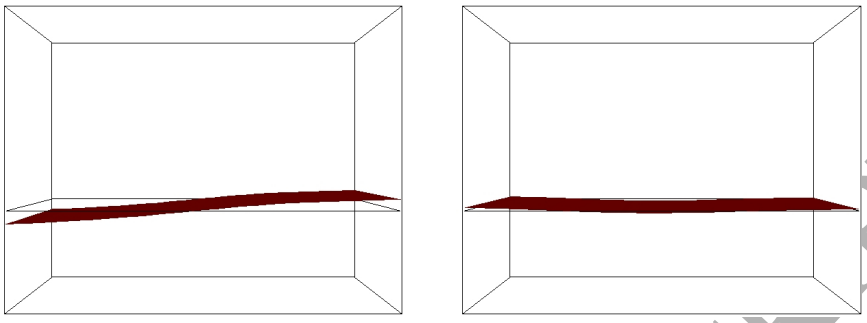

(a) Time $t = 83.63$ s (b) Time $t = 83.90$ s

Figure 12: Free surface evolution for the forced sloshing with $f = 0.87$ Hz solved with LS+BRCP.

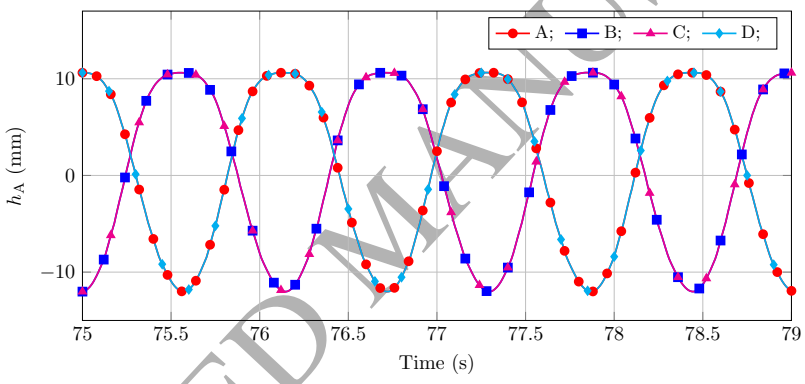

Figure 13: Forced sloshing with $f = 0.87$ Hz. Verification of the two-dimensional behaviour of the numerical results with level set.

volume control; however, the execution time must be doubled to reduce the volume variation from 9.1% in Case 2 to 3.6% in Case 3, which is not satisfactory due to the decrease in the position of the free surface, as shown in Fig. 14.

Furthermore, a mesh convergence study is performed with the volume variation taken as a parameter. As summarized in Table 2, less refined meshes, as in cases 4 and 5, lead to higher mass losses, while the same refinements solved with the volume-preserving algorithm, cases 6 and 7, respectively, show bounded mass loss. Note that the coarser the mesh, the higher the mass loss, with and

Case	C_{vol}	Δt [s]	h_{FS} [mm]	ΔV_{w}[%]
1 (ref)	0.1	0.01	3.5	< 0.2
2	0	0.01	3.5	9.1
3	0	0.005	3.5	3.6
4	0	0.01	7.0	31.5
5	0	0.01	4.7	16.0
6	0.1	0.01	7.0	< 1.15
7	0.1	0.01	4.7	< 0.7

Table 2: Percentage of volume variation for different space and time discretizations for the forced sloshing with f = 0.87 Hz.

without volume control. It should be mentioned that for cases 1, 6 and 7, with volume control, the maximum volume differences considered are registered at the end of the initial transient period and not at $t = 100$ s.

5.2.2. Sloshing with an imposed frequency of $f_2 = 2.10\,Hz$

It was verified experimentally that an imposed motion of 2.10 Hz induces 3D effects on the free surface displacements with an expected shape similar to the one represented in Fig. 15.

The 3D numerical domain represents the experimental work described in Sec. 5.1, and the measurements at points A, B, C and D, arranged as in Fig. 6, are chosen for comparison with numerical curves. Note that the measured amplitudes are higher than those in Sec. 5.2.1 and the period is shorter.

The horizontal acceleration with an amplitude of $A = 10$ mm in the $x-$direction is imposed from time $T = 0$ to approximately $T = 200$ s, and then the system enters free sloshing conditions. The displacements at the four sample points for the whole experiment are represented in Fig. 16. Figures 20(a) and 20(b) show the alternating displacements at the measurement points during two seconds of the experiment's time-periodic stage. Points A and C, which are arranged diagonally, rise and fall at the same time, as do points B and D. Therefore, the free surface in the tank shows 3D behaviour. Note that even though the

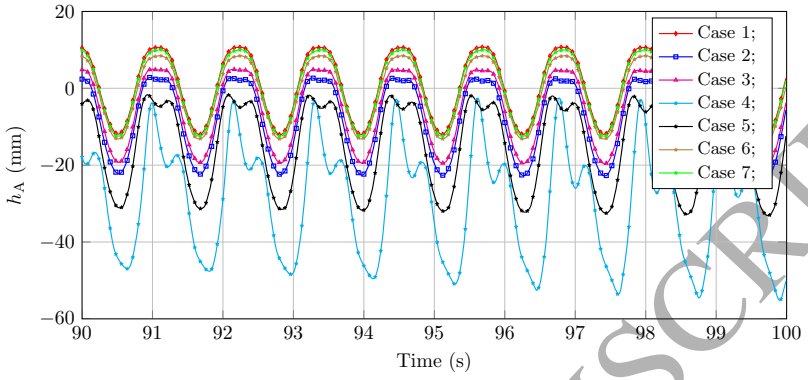

Figure 14: Forced sloshing with $f = 0.87\,\text{Hz}$. free surface displacements in sample A for the LS+BRCP algorithm for different cases.

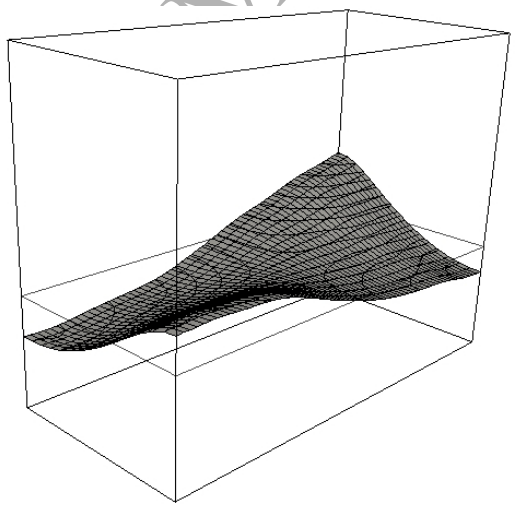

Figure 15: Forced sloshing with $f = 2.10\,\text{Hz}$. free surface shape near the inviscid mode $i = 1$, $j = 1$ numerically obtained.

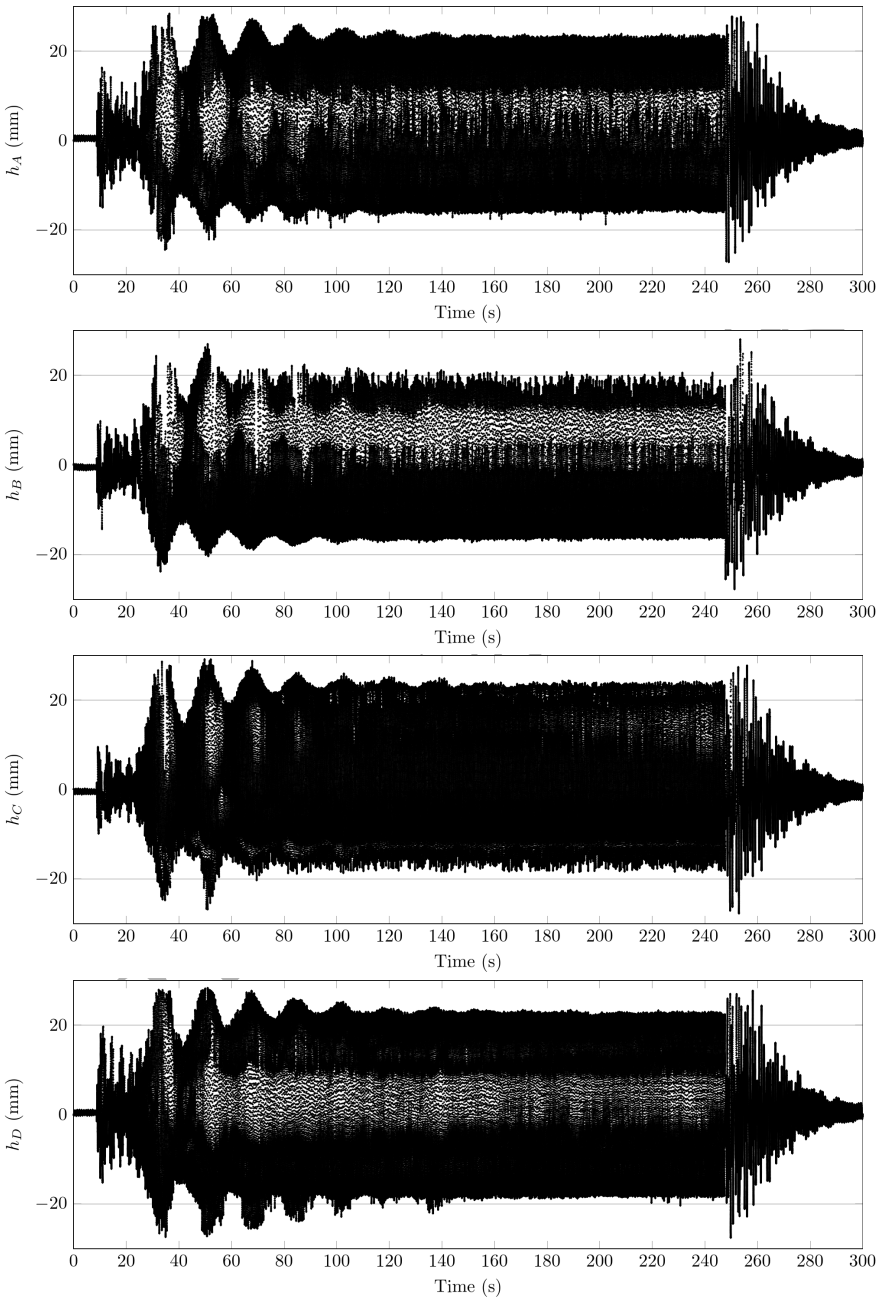

Figure 16: Forced sloshing with $f_2 = 2.10\,\mathrm{Hz}$. Experimental free surface displacements in sample points.

maximum (positive) displacements are similar for the four measurement points, the minimum (negative) amplitudes are lower for A and B than for C and D. This may be attributable to the sum of the two basic motion modes in each horizontal coordinate.

Numerical simulations were conducted using a time step of $\Delta t = 0.005$ s, with changes in the mesh with respect to the former case because the velocities registered in the present example are higher than those in the $f_1 = 0.87\,\mathrm{Hz}$ simulation. The discretization is in hexahedral elements, with 62 elements in the x-direction, 15 in the z-direction and 54 in the vertical y-direction. In this model, in the vertical direction, there are 8 layers of 0.0075 m on the bottom, 40 layers of 0.00318 m in the middle region, and 6 layers of 0.0188 m on top. For the turbulence model, $l_{\mathrm{mix}} = 0.15$ m for the mean element size and $\mu_{\max} = 0.15$ kg (m s)$^{-1}$ were adopted.

The LS+BRCP technique was solved with the following parameters: $M = 50000$, $\kappa = (3h_y)^2 = 1.1 \times 10^{-4}$ m^2 for the reinitialization, and $C_{\mathrm{vol}} = 0.1$ and $D_{\mathrm{vol}} = L_x\, L_z\, (3h_y) = 7.46 \times 10^{-4}$ m^3 for the volume-preserving algorithm.

The free surface initial position adopted for the simulation is a slightly inclined plane, with a maximum displacement of 0.5 mm with respect to the resting position in the yz plane, i.e., perpendicular to the horizontal acceleration direction. This initial condition was chosen due to the fact that, for the combination of symmetric initial conditions, symmetric mesh and symmetric excitation, no 3D effect is induced, and the experimental behaviour is not reproduced.

It has been observed that 3D behaviour is also promoted by a slight skewer (in the xz plane) horizontal acceleration and by using a non-regular 3D mesh. The results computed with all these options are in agreement with each other. Nevertheless, the option to modify the initial condition is less intrusive, because it is a slight initial perturbation that is independent of the discretization. The final results do not depend on the mechanism used to promote the 3D asymmetry. Note that if no perturbation is used, only symmetric (i.e., 2D) sloshing appears.

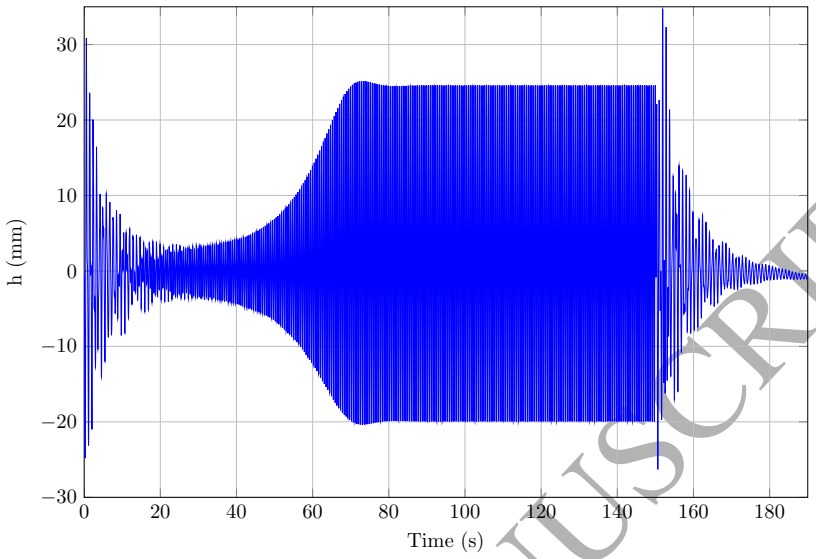

Figure 17: Forced sloshing with $f_2 = 2.10\,\text{Hz}$. Numerical free surface displacements in B.

The time evolution of the free surface displacement registered for sample B in the numerical simulations with LS+BRCP is represented in Fig. 17, where three stages are distinguished: an initial transient region in time interval $(0, 73$ s], a time-periodic stage from time $t = 73$ s to $t = 150$ s, and the decay period to the end of the study.

During the initial transient stage, free surface displacements of approximately 20% of the fluid depth are registered in sample B, as shown in Fig. 17. However, larger displacements of about 40% of the fluid depth are registered at positions where there are not experimental measurements, as seen in Fig. 18. Note that there are no breaking waves, even for this amount of free surface displacements, probably due to the ratio between the water depth and the tank's horizontal size. The vorticity and velocity vectors over a vertical plane at position $z = 0.025$ m are presented in Fig. 19 for the same time points as in the former picture. Vortices are not sufficiently developed to promote wave breaking, as presented in [38], where sloshing cases under roll excitation for a shallow water depth are studied. After the first steps, the free surface displacements

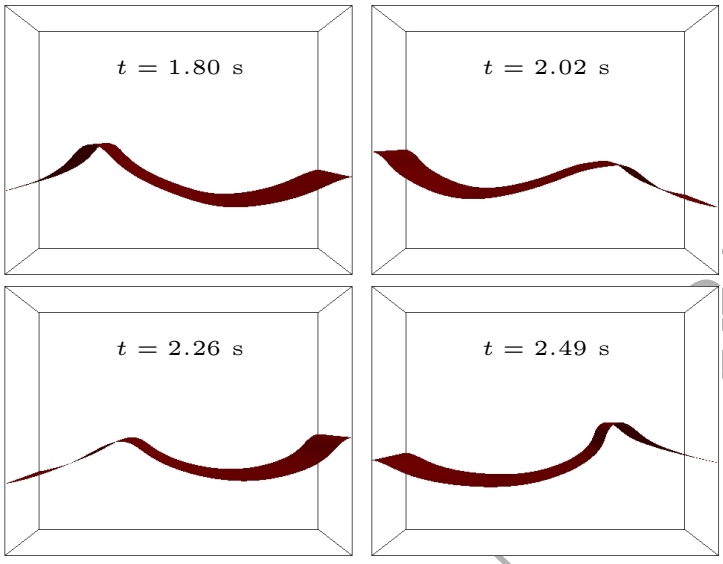

Figure 18: Forced sloshing with $f_2 = 2.10\,\text{Hz}$. free surface during the initial transient stage.

decay up to $t = 20$ s, when the 3D behaviour is established and the amplitudes start to grow. The time-periodic regime is established from $t \approx 73$ s.

For the time-periodic stage, the amplitudes and periods for the experimental and numerical measurements are given in Figs. 20(a) and 20(b) for two seconds. The previously mentioned effect for the experimental results is easily identified in the numerical plots: measurements at points A-C coincide in phase, as well as measurements at points B-D; however, the maximum and minimum amplitudes are slightly different. The numerical case shows that the absolute amplitudes are higher for points C and D than for A and B, respectively, and have more pronounced negative amplitudes. The snapshots from experimental videos and numerical simulations are presented in Fig. 21 for several instants. The free surface exhibits a complex 3D behaviour. From this figure, it is also apparent that the maximum amplitudes at points A and C (see Fig. 20(a)) occur at instants where minimum amplitudes are obtained for points B and D (see Fig. 20(b)).

The interface position and the vorticity and the velocity vectors for half a

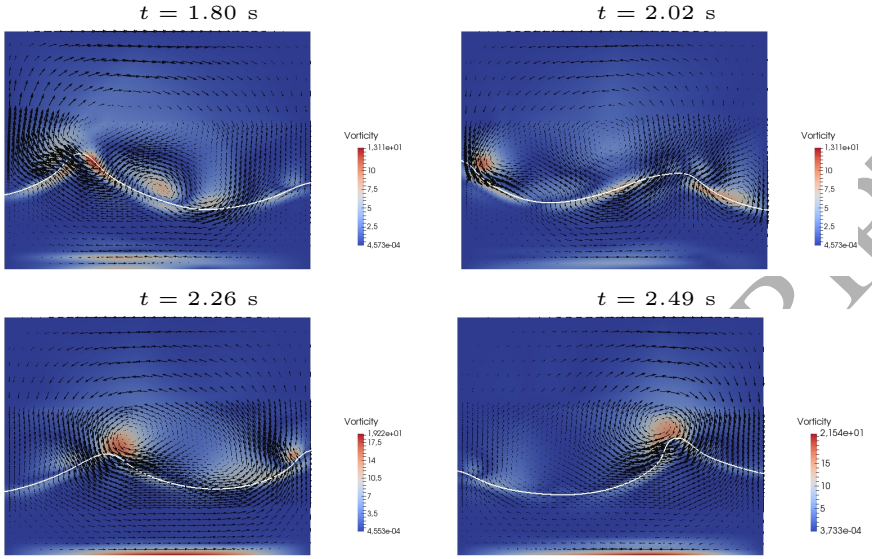

Figure 19: Forced sloshing with $f_2 = 2.10$ Hz. free surface profile, velocity vectors and vorticity in the vertical plane parallel to xy at $z = 0.025$ m during the initial transient stage.

period of the time-periodic movement are plotted for a vertical plane parallel to xy at $z = 0.025$ m in Fig. 22. The velocity vectors show vertical behaviour in regions near the wall, as well as a less curved free surface with respect to the initial transient regime.

During the decay period, which begins when horizontal acceleration is stopped at time $t = 150$ s, for the numerical simulation, the displacement of the free surface gradually reduces. The large displacements registered in Fig. 17, at times $t = 150.64$ s and $t = 151.91$ s for sample B, keep the shape of the movement of the time-periodic stage, i.e., the interface does not suffer breaking up or folding.

In addition, a fast Fourier transform (FFT) spectral analysis of the experimental and numerical signals confirms the relevant frequencies. The imposed frequency appears during the initial transient and time-periodic regimes. A frequency of 1.13 Hz, close to the theoretical primary resonance (mode (1,0)), is clearly observed during the free-sloshing regime. In such regime, frequencies of 2.10 Hz and 2.43 Hz are also identified.

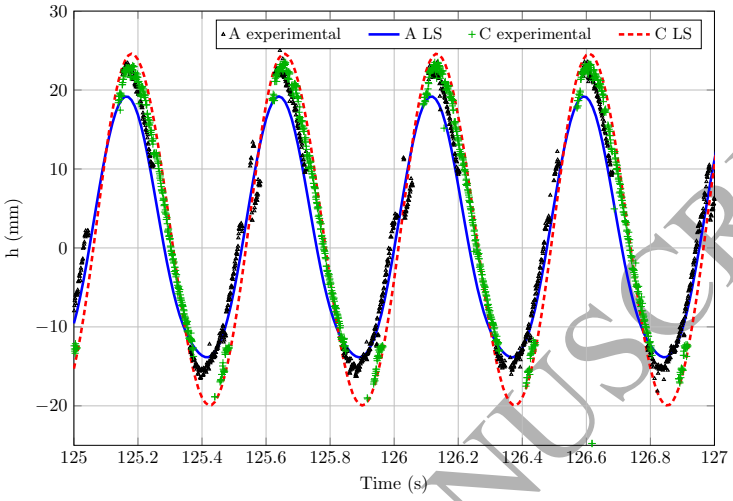

(a) Points A and C

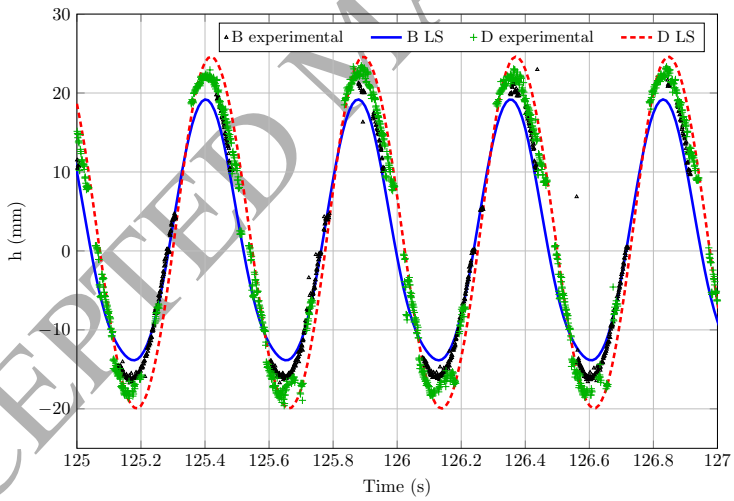

(b) Points B and D

Figure 20: Forced sloshing with $f_2 = 2.10\,\text{Hz}$. free surface displacements measured experimentally and determined numerically.

6. Conclusions

Within the context of a two-fluid flow field-stabilized finite element method, a level set technique with bounded renormalization and continuous penalization has been improved with a 3D volume-preserving algorithm that avoids the unphysical loss of mass for the results of long time simulations.

In addition, the experimental results for a forced sloshing problem have been reported. Imposed motions with different amplitudes and frequencies are studied to evaluate the evolution of 3D free surface behaviour. The 3D numerical analyses of the experiments are focused on the description of a 2D planar mode and a fully 3D behaviour mode.

The numerical formulation was first verified by simulating free-sloshing laminar cases. Their results satisfactorily match the analytical solution for deep two-fluid flows, as well as a solution obtained with a different numerical method, MLIRT. The effectiveness of the volume-preserving algorithm has been evaluated with two different time discretizations, with and without volume control, showing that the differences in wave amplitude are larger than the differences in volume change. The results obtained for shallow two-fluid free sloshing are compared with those of a different numerical technique, providing a good comparison. In addition, the influence of depth in the wave evolution is well described.

The 3D numerical performance of the formulation was validated by comparing the numerical predictions during the forced sloshing time-periodic regime with experimental data. The computed wave height evolution matches the experimental data for the cases analysed.

The free surface description at $f_1 = 0.87\,\mathrm{Hz}$, confirms that the results obtained using the 3D model agree with those obtained using 2D models. The volume-preserving algorithm was tested with different time steps and space discretizations, showing mesh convergence for both cases, i.e., with and without the mass-preserving strategy. Furthermore, when no volume-preserving algorithm is applied, the mesh and time refinements would lead to extremely expensive

numerical models to obtain acceptable results in terms of free surface displacement.

The 3D effects observed from the forced sloshing experiments are accurately captured by the simulations at frequency of $f_2 = 2.10\,\mathrm{Hz}$. In particular, the effect of the initial conditions has been found to be relevant for capturing the 3D effects. Different stages have been identified throughout the experimental and numerical analyses: an initial transient stage, a time periodic stage and a free decay stage. The initial transient free surface displacements are highly nonlinear, though without wave breaking, and constitute a challenge for the numerical method when predicting the interface behaviour. The following stage, the time-periodic regime, is well captured for the level set technique, showing quasi-sinusoidal profiles in the free surfaces. Finally, the free decay period maintains the free surface shapes of the previous period but with lower amplitudes.

As a result, the formulation for the two-fluid finite element method with a volume-preserving algorithm coupled to the bounded renormalization with continuous penalization for a level set has shown good behaviour for describing 3D sloshing problems of air-water systems with free surface displacements from 20 to 40% of the water depth and is well suited for long-term simulations.

7. Acknowledgements

The authors are grateful for the support provided by various research projects: Chilean Council for Scientific and Technological Research (CONICYT) (FONDECYT grant 1170620); the Scientific Research Projects Management Department of the Vice Presidency of Research, Development and Innovation (DICYT-VRID) of the Universidad de Santiago de Chile (grant Proyecto Basal USA1555 - Vridei O51716CSSSA); RED CYTED 516RT0512 High Performance Computing in Engineering, Iberoamerican Scientific and Technological Development Program (CYTED, in Spanish); Argentinian Council for Scientific Research (CONICET) (grant PIP-11220150100588CO); Argentinian Fund for Scientific Research and Technology (FONCyT) (grants PICT-0938-2013, PICT-2660-2014,

PICT-2015-2904, PME-2015-0036); Santa Fe STI Agency (grant 00010-18-2014); Argentinian Ministry of Defence (grant PIDDEF-4/14); Universidad Tecnológica Nacional (grant PID-3526), and Universidad Nacional del Litoral (grant CAI+D 501-201101-00233). The authors made extensive use of Free Software including GNU/Linux OS, GCC compilers, and Octave, and Open Source software including ParaView.

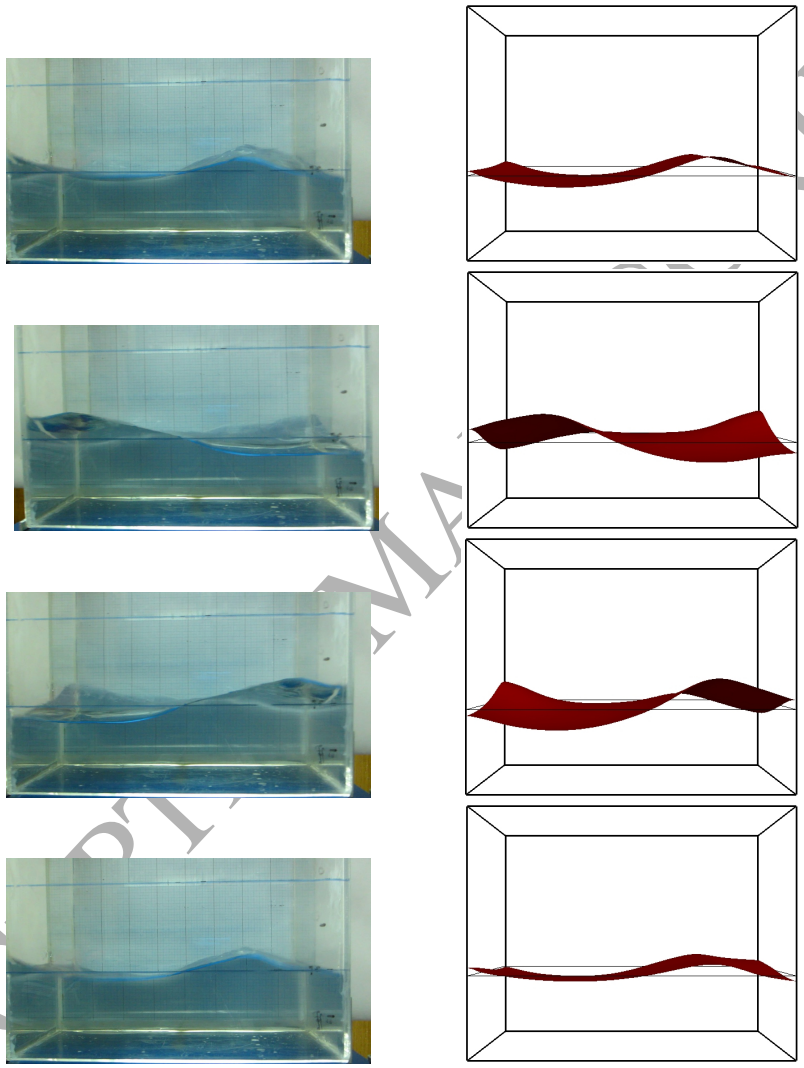

Figure 21: Free surface evolution for $f = 2.10$ Hz during the time-periodic stage: experiment snapshots on the left; numerical results on the right.

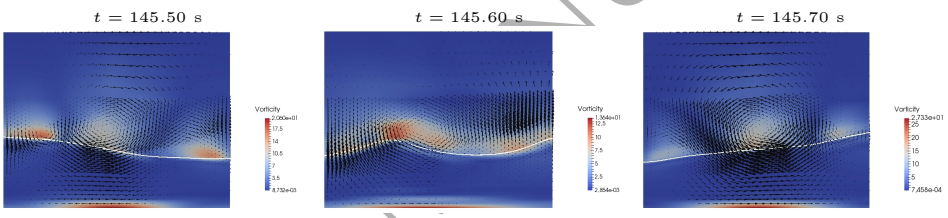

Figure 22: Forced sloshing with $f_2 = 2.10$ Hz. free surface profile, velocity vectors and vorticity in the vertical plane parallel to xy at $z = 0.025$ m in the time-periodic stage.

References

References

[1] M. Lazzarin, M. Biolo, A. Bettella, M. Manente, R. D. Forno, D. Pavarin, EUCLID Satellite: Sloshing model development through computational fluid dynamics, Aerospace Science and Technology 36 (2014) 44 – 54. doi:10.1016/j.ast.2014.03.015.

[2] H. Hernández-Barrios, E. Heredia-Zavoni, A. A. Aldama-Rodríguez, Nonlinear sloshing response of cylindrical tanks subjected to earthquake ground motion, Engineering Structures 29 (12) (2007) 3364 – 3376. doi:10.1016/j.engstruct.2007.08.023.

[3] I. Gejadze, G. Copeland, Open boundary control problem for Navier-Stokes equations including a free surface: Adjoint sensitivity analysis, Computers & Mathematics with Applications 52 (89) (2006) 1243–1268. doi:10.1016/j.camwa.2006.11.004.

[4] M. Marivani, M. Hamed, Numerical study of slat screen pattern effect on design parameters of tuned liquid dampers, ASME Journal of Fluids Engineering 136 (6) (2014) 061201–061201–11. doi:10.1115/1.4026662.

[5] A. Marsh, M. Prakash, E. Semercigil, Ö. F. Turan, A numerical investigation of energy dissipation with a shallow depth sloshing absorber, Applied Mathematical Modelling 34 (10) (2010) 2941–2957. doi:10.1016/j.apm.2010.01.004.

[6] J. B. Frandsen, Sloshing motions in excited tanks, Journal of Computational Physics 196 (1) (2004) 53–87. doi:10.1016/j.jcp.2003.10.031.

[7] R. Ibrahim, Liquid Sloshing Dynamics: Theory and Applications, Vol. 1, 2005. doi:10.1017/CBO9781107415324.004.

[8] O. M. Faltinsen, O. F. Rognebakke, A. N. Timokha, Classification of three-dimensional nonlinear sloshing in a square-base tank with finite depth,

Journal of Fluids and Structures 20 (1) (2005) 81–103. doi:10.1016/j.jfluidstructs.2004.08.001.

[9] D. Liu, P. Lin, A numerical study of three-dimensional liquid sloshing in tanks, Journal of Computational Physics 227 (8) (2008) 3921–3939. doi:10.1016/j.jcp.2007.12.006.

[10] O. Faltinsen, A. Timokha, Undamped eigenperiods of a sea-based gravity monotower, Applied Mathematical Modelling 40 (19) (2016) 8217–8243. doi:10.1016/j.apm.2016.04.003.

[11] O. M. Faltinsen, O. F. Rognebakke, I. a. Lukovsky, A. N. Timokha, Multidimensional modal analysis of nonlinear sloshing in a rectangular tank with finite water depth, Journal of Fluid Mechanics 407 (2000) 201–234. doi:10.1017/S0022112099007569.

[12] O. M. Faltinsen, A. N. Timokha, Asymptotic modal approximation of nonlinear resonant sloshing in a rectangular tank with small fluid depth, Journal of Fluid Mechanics 470 (2002) 319–357. doi:10.1017/S0022112002002112.

[13] O. M. Faltinsen, A. N. Timokha, A multimodal method for liquid sloshing in a two-dimensional circular tank, Journal of Fluid Mechanics 665 (2010) 457–479. doi:10.1017/S002211201000412X.

[14] N. Vaziri, M.-J. Chern, A. G. Borthwick, Effects of base aspect ratio on transient resonant fluid sloshing in a rectangular tank: A numerical study, Ocean Engineering 105 (2015) 112–124. doi:10.1016/j.oceaneng.2015.06.020.

[15] A. Kalogirou, E. E. Moulopoulou, O. Bokhove, Variational finite element methods for waves in a Hele-Shaw tank, Applied Mathematical Modelling 40 (17) (2016) 7493–7503. doi:10.1016/j.apm.2016.02.036.

[16] R. Löhner, C. Yang, E. Oñate, On the simulation of flows with violent free surface motion, Computer Methods in Applied Mechanics and Engineering 195 (41–43) (2006) 5597–5620. doi:10.1016/j.cma.2005.11.010.

[17] H. Akyildız, N. E. Ünal, Sloshing in a three-dimensional rectangular tank: numerical simulation and experimental validation, Ocean Engineering 33 (16) (2006) 2135–2149. doi:10.1016/j.oceaneng.2005.11.001.

[18] O. Oxtoby, A. Malan, J. Heyns, A computationally efficient 3D finite-volume scheme for violent liquid–gas sloshing, International Journal for Numerical Methods in Fluids 79 (6) (2015) 306–321. doi:10.1002/fld.4055.

[19] T. Nagashima, Sloshing analysis of a liquid storage container using level set X-FEM, Communications in Numerical Methods in Engineering 25 (4) (2009) 357–379. doi:10.1002/cnm.1122.

[20] R. F. Ausas, E. A. Dari, G. C. Buscaglia, A geometric mass-preserving redistancing scheme for the level set function, International Journal for Numerical Methods in Fluids 65 (8) (2011) 989–1010. doi:10.1002/fld.2227.

[21] A. Huerta, W. K. Liu, Viscous flow with large free surface motion, Computer Methods in Applied Mechanics and Engineering 69 (3) (1988) 277–324. doi:10.1016/0045-7825(88)90044-8.

[22] L. Battaglia, J. D'Elía, M. Storti, Simulación numérica de la agitación en tanques de almacenamiento de líquidos mediante una estrategia lagrangiana euleriana arbitraria, Revista Internacional de Métodos Numéricos para Cálculo y Diseño en Ingeniería 28 (2) (2012) 124–134. doi:10.1016/j.rimni.2012.02.001.

[23] M. A. Cruchaga, R. S. Reinoso, M. A. Storti, D. J. Celentano, T. E. Tezduyar, Finite element computation and experimental validation of sloshing in rectangular tanks, Computational Mechanics 52 (6) (2013) 1301–1312. doi:10.1007/s00466-013-0877-0.

[24] T. E. Tezduyar, Finite elements in fluids: stabilized formulations and moving boundaries and interfaces, Computers & Fluids 36 (2) (2007) 191–206. doi:10.1016/j.compfluid.2005.02.011.

[25] C.-H. Wu, B.-F. Chen, T.-K. Hung, Hydrodynamic forces induced by transient sloshing in a 3D rectangular tank due to oblique horizontal excitation, Computers & Mathematics with Applications 65 (8) (2013) 1163–1186. doi:10.1016/j.camwa.2013.02.012.

[26] A. Rafiee, F. Pistani, K. Thiagarajan, Study of liquid sloshing: numerical and experimental approach, Computational Mechanics 47 (1) (2011) 65–75. doi:10.1007/s00466-010-0529-6.

[27] J. M. Gimenez, L. M. González, An extended validation of the last generation of particle finite element method for free surface flows, Journal of Computational Physics 284 (2015) 186–205. doi:10.1016/j.jcp.2014.12.025.

[28] C. Zhang, Y. Li, Q. Meng, Fully nonlinear analysis of second-order sloshing resonance in a three-dimensional tank, Computers & Fluids 116 (2015) 88–104. doi:10.1016/j.compfluid.2015.04.016.

[29] S. Elgeti, H. Sauerland, Deforming fluid domains within the finite element method: Five mesh-based tracking methods in comparison, Archives of Computational Methods in Engineering 23 (2) (2016) 323–361. doi:10.1007/s11831-015-9143-2.

[30] M. Sussman, E. G. Puckett, A coupled level set and volume-of-fluid method for computing 3D and axisymmetric incompressible two-phase flows, Journal of Computational Physics 162 (2) (2000) 301–337. doi:10.1006/jcph.2000.6537.

[31] X. Yang, A. J. James, J. Lowengrub, X. Zheng, V. Cristini, An adaptive coupled level-set/volume-of-fluid interface capturing method for unstruc-

tured triangular grids, Journal of Computational Physics 217 (2) (2006) 364–394. doi:10.1016/j.jcp.2006.01.007.

[32] X. Lv, Q. Zou, Y. Zhao, D. Reeve, A novel coupled level set and volume of fluid method for sharp interface capturing on 3D tetrahedral grids, Journal of Computational Physics 229 (7) (2010) 2573–2604. doi:10.1016/j.jcp.2009.12.005.

[33] Y. Zhao, H.-C. Chen, Numerical simulation of 3D sloshing flow in partially filled LNG tank using a coupled level-set and volume-of-fluid method, Ocean Engineering 104 (2015) 10–30. doi:10.1016/j.oceaneng.2015.04.083.

[34] D. Enright, F. Losasso, R. Fedkiw, A fast and accurate semi-Lagrangian particle level set method, Computers & Structures 83 (67) (2005) 479–490. doi:10.1016/j.compstruc.2004.04.024.

[35] V. Le Chenadec, H. Pitsch, A 3D unsplit forward/backward volume-of-fluid approach and coupling to the level set method, Journal of Computational Physics 233 (1) (2013) 10–33. doi:10.1016/j.jcp.2012.07.019.

[36] S. Shin, D. Juric, A hybrid interface method for three-dimensional multiphase flows based on front tracking and level set techniques, International Journal for Numerical Methods in Fluids 60 (7) (2009) 753–778. doi:10.1002/fld.1912.

[37] C.-H. Wu, O. M. Faltinsen, B.-F. Chen, Numerical study of sloshing liquid in tanks with baffles by time-independent finite difference and fictitious cell method, Computers & Fluids 63 (2012) 9 – 26. doi:10.1016/j.compfluid.2012.02.018.

[38] E. L. Grotle, H. Bihs, V. Æsøy, Experimental and numerical investigation of sloshing under roll excitation at shallow liquid depths, Ocean Engineering 138 (Supplement C) (2017) 73 – 85. doi:10.1016/j.oceaneng.2017.04.021.

[39] M. Sussman, P. Smereka, S. Osher, A level set approach for computing solutions to incompressible two-phase flow, Journal of Computational Physics 114 (1) (1994) 146–159. doi:10.1006/jcph.1994.1155.

[40] M. Cruchaga, L. Battaglia, M. Storti, J. D'Elía, Numerical modeling and experimental validation of free surface flow problems, Archives of Computational Methods in Engineering 23 (1) (2016) 139–169. doi:10.1007/s11831-014-9138-4.

[41] M. Sussman, E. Fatemi, An efficient, interface-preserving level set redistancing algorithm and its application to interfacial incompressible fluid flow, SIAM Journal on Scientific Computing 20 (4) (1999) 1165–1191. doi:10.1137/S1064827596298245.

[42] H. Kohno, T. Tanahashi, Numerical analysis of moving interfaces using a level set method coupled with adaptive mesh refinement, International Journal for Numerical Methods in Fluids 45 (9) (2004) 921–944. doi:10.1002/fld.715.

[43] S. Kurioka, D. R. Dowling, Numerical simulation of free surface flows with the level set method using an extremely high-order accuracy WENO advection scheme, International Journal of Computational Fluid Dynamics 23 (3) (2009) 233–243. doi:10.1080/10618560902776786.

[44] E. Olsson, G. Kreiss, S. Zahedi, A conservative level set method for two phase flow II, Journal of Computational Physics 225 (1) (2007) 785–807. doi:10.1016/j.jcp.2006.12.027.

[45] L. Zhao, J. Mao, X. Bai, X. Liu, T. Li, J. Williams, Finite element implementation of an improved conservative level set method for two-phase flow, Computers & Fluids 100 (2014) 138 – 154. doi:10.1016/j.compfluid.2014.04.027.

[46] M. A. Cruchaga, D. J. Celentano, T. E. Tezduyar, Moving-interface computations with the edge-tracked interface locator technique (ETILT), Inter-

national Journal for Numerical Methods in Fluids 47 (6-7) (2005) 451–469. doi:10.1002/fld.825.

[47] L. Battaglia, M. A. Storti, J. D'Elía, Bounded renormalization with continuous penalization for level set interface-capturing methods, International Journal for Numerical Methods in Engineering 84 (7) (2010) 830–848. doi:10.1002/nme.2925.

[48] L. Battaglia, M. A. Storti, J. D'Elía, Simulation of free-surface flows by a finite element interface capturing technique, International Journal of Computational Fluid Dynamics 24 (3-4) (2010) 121–133. doi:10.1080/10618562.2010.495695.

[49] M. Cruchaga, D. Celentano, P. Breitkopf, P. Villon, A. Rassineux, A front remeshing technique for a Lagrangian description of moving interfaces in two-fluid flows, International Journal for Numerical Methods in Engineering 66 (13) (2006) 2035–2063. doi:10.1002/nme.1616.

[50] M. Cruchaga, D. Celentano, P. Breitkopf, P. Villon, A. Rassineux, A surface remeshing technique for a Lagrangian description of 3D two-fluid flow problems, International Journal for Numerical Methods in Fluids 63 (4) (2010) 415–430. doi:10.1002/fld.2073.

[51] A. N. Brooks, T. J. Hughes, Streamline upwind/Petrov-Galerkin formulations for convection dominated flows with particular emphasis on the incompressible Navier-Stokes equations, Computer Methods in Applied Mechanics and Engineering 32 (13) (1982) 199–259. doi:10.1016/0045-7825(82)90071-8.

[52] L. Battaglia, J. D'Elía, M. A. Storti, Computational Fluid Dynamics: Theory, Analysis and Applications, Nova Science Publishers, 2011, Ch. Numerical approaches for solving free surface fluid flows, pp. 351–384, ISBN: 978-1-61209-276-8.

[53] M. A. Cruchaga, E. Oñate, A generalized streamline finite element approach for the analysis of incompressible flow problems including moving surfaces, Computer Methods in Applied Mechanics and Engineering 173 (12) (1999) 241–255. doi:10.1016/S0045-7825(98)00272-2.

[54] E. Olsson, G. Kreiss, A conservative level set method for two phase flow, Journal of Computational Physics 210 (1) (2005) 225–246. doi:10.1016/j.jcp.2005.04.007.

[55] C. Kees, I. Akkerman, M. Farthing, Y. Bazilevs, A conservative level set method suitable for variable-order approximations and unstructured meshes, Journal of Computational Physics 230 (12) (2011) 4536–4558. doi:10.1016/j.jcp.2011.02.030.

[56] M. Owkes, O. Desjardins, A discontinuous Galerkin conservative level set scheme for interface capturing in multiphase flows, Journal of Computational Physics 249 (0) (2013) 275–302. doi:10.1016/j.jcp.2013.04.036.

[57] M. A. Cruchaga, D. J. Celentano, T. E. Tezduyar, Computational modeling of the collapse of a liquid column over an obstacle and experimental validation, Journal of Applied Mechanics - Transactions of the ASME 76 (2) (2009) 0212021–021205. doi:10.1115/1.3057439.

[58] A. Prosperetti, Motion of two superposed viscous fluids, Physic of Fluids 24 (7) (1981) 1217–1223. doi:10.1063/1.863522.

[59] T. Tezduyar, M. Behr, S. Mittal, J. Liou, A new strategy for finite element computations involving moving boundaries and interfaces – The deforming-spatial-domain/space-time procedure: II. Computation of free-surface flows, two-liquid flows, and flows with drifting cylinders., Computer Methods in Applied Mechanics and Engineering 94 (3) (1992) 353–371. doi:10.1016/0045-7825(92)90060-W.

[60] M. A. Cruchaga, E. Oñate, A finite element formulation for incompressible flow problems using a generalized streamline operator, Computer Methods

in Applied Mechanics and Engineering 143 (12) (1997) 49–67. doi:10.1016/S0045-7825(97)84579-3.

[61] O. M. Faltinsen, O. F. Rognebakke, A. N. Timokha, Resonant three-dimensional nonlinear sloshing in a square-base basin, Journal of Fluid Mechanics 487 (2003) 142. doi:10.1017/S0022112003004816.

[62] D. Liu, W. Tang, J. Wang, H. Xue, K. Wang, Comparison of laminar model, RANS, LES and VLES for simulation of liquid sloshing, Applied Ocean Research 59 (C) (2016) 638 – 649. doi:10.1016/j.apor.2016.07.012.

[63] P. A. Caron, M. A. Cruchaga, A. E. Larreteguy, Sensitivity analysis of finite volume simulations of a breaking dam problem, International Journal of Numerical Methods for Heat & Fluid Flow 25 (7) (2015) 1718–1745. doi:10.1108/HFF-10-2014-0308.

[64] M. A. Cruchaga, D. J. Celentano, T. E. Tezduyar, Collapse of a liquid column: Numerical simulation and experimental validation, Computational Mechanics 39 (4) (2007) 453–476. doi:10.1007/s00466-006-0043-z.

[65] R. S. Reinoso, Análisis del comportamiento 3D en el problema de agitación de líquidos en contenedores, Master's thesis, Universidad de Santiago de Chile (USACH), Chile, in Spanish (2012).